

INTERACTION OF ELECTROMAGNETIC FIELDS WITH BIOSYNTHETIC PROCESSES IN CONNECTIVE TISSUE CELLS

Alan J. Grodzinsky, Ph.D.
Michael D. Buschmann, M.S.
Yehezkiel A. Gluzband, M.S.

Massachusetts Institute of Technology
Cambridge, MA 02139

December 1990

Final Report for Period May 1989 - April 1990

Approved for public release; distribution is unlimited.

Prepared for
USAF SCHOOL OF AEROSPACE MEDICINE
Human Systems Division (AFSC)
Brooks Air Force Base, TX 78235-5301



91 4 04 010

Notices


This final report was submitted by the Laboratory for Electromagnetic and Electronic Systems, Department of Electrical Engineering and Computer Science, Massachusetts Institute of Technology, Cambridge, Massachusetts, under contract F33615-87-D-0609, Task #SCEEE-AFB/89-0024, job order 2312-W1-14 with the USAF School of Aerospace Medicine, Human Systems Division, AFSC, Brooks Air Force Base, Texas. Dr. Johnathan L. Kiel (USAFSAM/RZP) was the Laboratory Project Scientist-in-Charge.


When Government drawings, specifications, or other data are used for any purpose other than in connection with a definitely Government-related procurement, the United States Government incurs no responsibility nor any obligation whatsoever. The fact that the Government may have formulated or in any way supplied the said drawings, specifications, or other data, is not to be regarded by implication, or otherwise in any manner construed, as licensing the holder, or any other person or corporation; or as conveying any rights or permission to manufacture, use, or sell any patented invention that may in way be related thereto.

The animals involved in this study were procured, maintained, and used in accordance with the Animal Welfare Act and the "Guide for the Care and Use of Laboratory Animals" prepared by the Institute of Laboratory Animal Resources - National Research Council.

The Office of Public Affairs has reviewed this report, and it is releasable to the National Technical Information Service, where it will be available to the general public, including foreign nationals.

This report has been reviewed and is approved for publication.


JOHNATHAN L. KIEL, Ph.D.
Project Scientist


DAVID N. ERWIN, Ph.D.
Supervisor


GEORGE E. SCHWENDER, Colonel, USAF, MC, CFS
Commander

UNCLASSIFIED

SECURITY CLASSIFICATION OF THIS PAGE

REPORT DOCUMENTATION PAGE				Form Approved OMB No. 0704-0183	
1a. REPORT SECURITY CLASSIFICATION Unclassified			1b. RESTRICTIVE MARKINGS		
2a. SECURITY CLASSIFICATION AUTHORITY			3. DISTRIBUTION/AVAILABILITY OF REPORT Approved for public release; distribution is unlimited.		
2b. DECLASSIFICATION/DOWNGRADING SCHEDULE					
4. PERFORMING ORGANIZATION REPORT NUMBER(S)			5. MONITORING ORGANIZATION REPORT NUMBER(S) USAFSAM-TR-90-27		
6a. NAME OF PERFORMING ORGANIZATION Massachusetts Institute of Technology		6b. OFFICE SYMBOL (if applicable)	7a. NAME OF MONITORING ORGANIZATION USAF School of Aerospace Medicine (R7P)		
6c. ADDRESS (City, State, and ZIP Code) Department of Electrical Engineering & Computer Science, Rm. 38-377 Massachusetts Institute of Technology Cambridge, MA 02139		7b. ADDRESS (City, State, and ZIP Code) Human Systems Division (AFSC) Brooks AFB, TX 78235-5301			
8a. NAME OF FUNDING/SPONSORING ORGANIZATION		8b. OFFICE SYMBOL (if applicable)	9. PROCUREMENT INSTRUMENT IDENTIFICATION NUMBER F33615-87-D-0609 Task 0024		
8c. ADDRESS (City, State, and ZIP Code)		10. SOURCE OF FUNDING NUMBERS			
		PROGRAM ELEMENT NO 61102F	PROJECT NO 2312	TASK NO W1	WORK UNIT ACCESSION NO 14
11. TITLE (Include Security Classification) Interaction of Electromagnetic Fields With Biosynthetic Processes in Connective Tissue Cells					
12. PERSONAL AUTHOR(S) Grodzinsky, Alan J.; Buschmann, Michael, D.; Gluzband, Yehezkiel, A.					
13a. TYPE OF REPORT Final		13b. TIME COVERED FROM 89/5/31 to 90/4/30		14. DATE OF REPORT (Year, Month, Day) 1990, December	
15. PAGE COUNT 58					
16. SUPPLEMENTARY NOTATION					
17. COSATI CODES			18. SUBJECT TERMS (Continue on reverse if necessary and identify by block number)		
FIELD	GROUP	SUB-GROUP	Radiobiology; Radiation biology; Electromagnetic fields; Radiofrequency wave propagation		
06	07				
20	14				
19. ABSTRACT (Continue on reverse if necessary and identify by block number) The specific objectives of this research period were (1) determine whether chondrocytes can be maintained in long-term (2-3 months) culture in agarose gel in order to test the effects of chronic as well as acute response to exposure to electromagnetic fields; (2) measure chondrocyte proliferation, biosynthetic rates for proteoglycans and proteins, total accumulation of proteoglycans, and physical properties of agarose/chondrocyte gel cultures; (3) construct specialized chambers for application of electric fields to agarose/chondrocyte disks in a standard incubator environment; and (4) begin experiments to measure the effects of applied current densities over a wide range of amplitudes and frequencies on biosynthesis of proteoglycans and proteins.					
20. DISTRIBUTION/AVAILABILITY OF ABSTRACT <input checked="" type="checkbox"/> UNCLASSIFIED/UNLIMITED <input type="checkbox"/> SAME AS RPT <input type="checkbox"/> DTIC USERS			21. ABSTRACT SECURITY CLASSIFICATION Unclassified		
22a. NAME OF RESPONSIBLE INDIVIDUAL Johnathan L. Kiel			22b. TELEPHONE (Include Area Code) (512) 536-3583		22c. OFFICE SYMBOL USAFSAM/RZP

INSPECTION
CO
DATE

SECRET
Distribution
Justification
Ex
Distribution
Availability
Dist Special
A-1
..... 1

INTRODUCTION	1
Articular Cartilage	1
Chondrocytes Cultured in Agarose	2
Continuum Models of the Physical Properties of Cartilage Matrix .	3
Macrocontinuum Theories	4
Microcontinuum Theories	5
CHONDROCYTES IN AGAROSE.....	6
Summary	6
Methods	7
Results and Discussion	10
Normal Chondrocytes	10
Swarm Rat Chondrosarcoma Cells	15
Conclusions	19
MODEL OF EQUILIBRIUM PROPERTIES.....	20
Summary	20
Introduction	20
Numerical Solution of the Poisson-Boltzmann Equation	22
Electrostatic Swelling Pressure in the Unit Cell	26
Comparison to Chondroitin Sulfate Solutions	29
Comparison to the Equilibrium Modulus of Articular Cartilage	37
EFFECT OF APPLIED ELECTRIC FIELDS.....	39
Experimental	39
REFERENCES.....	44
APPENDIX CARTILAGE PARAMETERS.....	51
Cartilage Constituent Compartments.....	51
Strain in GAG Compartment.....	52

SUMMARY

The interaction of electromagnetic fields with biological tissues is of increasing importance from the standpoint of potential health hazards and of possible beneficial (e.g., diagnostic and therapeutic) effects. To address these issues, the research accomplished during this period focused on the biosynthesis, assembly, and catabolism of highly specialized protein and polysaccharide molecules by mammalian connective tissue cells. Since the synthesis and processing of these macromolecules is one of the most important biological functions of connective tissue cells, altered matrix metabolism is known to be a most sensitive indicator of the effectiveness of an environmental stimulus, and of the pathway by which the stimulus evokes a response.

The long-term goal is to study long-term (*chronic*) and short-term (*acute*) effects of electromagnetic field exposure on the synthesis and turnover of highly charged proteoglycan (PG) molecules and their glycosaminoglycan (GAG) constituents, collagens, and other non-collagenous proteins by normal cartilage cells (chondrocytes) extracted from articular cartilage, and in rat chondrosarcoma cells (a continuous cell line). Another long-term goal is to study the possible role of fields in stimulating growth factor synthesis, and the combined role of fields and growth factors on chondrocyte metabolism.

To address these goals, the specific objectives of this research period were: (1) determine whether chondrocytes can be maintained in long-term agarose culture, in order to allow experiments involving chronic exposure to fields; (2) quantify chondrocyte proliferation, proteoglycan and protein biosynthetic rates, total proteoglycan accumulation, and matrix physical properties during long-term culture; (3) construct a special chamber to enable application of electric fields to agarose/chondrocyte disks maintained in culture in a standard incubator; and (4) begin electrical stimulation experiments over a range of current density amplitudes.

INTERACTION OF ELECTROMAGNETIC FIELDS WITH BIOSYNTHETIC PROCESSES IN CONNECTIVE TISSUE CELLS

INTRODUCTION

Articular Cartilage

Articular cartilage is the dense connective tissue that functions as a bearing material in synovial joints. Adult articular cartilage is avascular, aneural, and alymphatic; cell nutrition is derived primarily from the synovial fluid [1]. The chondrocytes are responsible for the synthesis, maintenance, and gradual turnover of an extracellular matrix (ECM) composed principally of a hydrated collagen fibril network enmeshed in a gel of highly charged proteoglycan molecules (PG). The composition and architecture of the matrix [2] and the tissue's high water content (70-80% of wet weight) enable cartilage to withstand complex compressive, tensile and shear deformation in joints [3, 4].

Cartilage ECM can remodel to meet the functional demands of loading. It is known, for example, that electrostatic and osmotic interactions between the proteoglycan constituents of the ECM enable cartilage to resist compressive loads [2, 5]. Animal studies have shown that PG content is higher in cartilage that is habitually loaded [6], while immobilization of joints leads to a decrease in PG synthesis and total PG content [7]. Osteoarthritic cartilage initially shows enhanced matrix synthesis in an apparent attempt to replace degraded PG molecules that have diffused out of the tissue. The mechanisms that mediate the biological response to mechanical loads are not understood.

Biosynthesis, metabolism, and turnover of cartilage matrix components have been studied extensively *in vivo* and using cell and tissue culture models [8]. Recent *in vitro* studies have shown that mechanical loads can also induce metabolic responses in cartilage organ cultures. Static compression has been found to decrease proteoglycan and protein synthesis [9, 10, 11], while dynamic compression at certain frequencies

and amplitudes stimulated synthesis of these matrix constituents [11]. Taken together, these data suggest that the presence of physiologic mechanical loading forces may be necessary for the proper assembly and maintenance of a matrix that can function in the joint.

Chondrocytes Cultured in Agarose

Investigators have recently found that bovine [12, 13, 14], rabbit [15], and human [16] chondrocytes as well as Swarm rat chondrosarcoma cells [17] isolated and cultured in agarose gel maintain their phenotype as evidenced by the synthesis of type II collagen and large aggregating proteoglycans. The newly synthesized macromolecules are effectively trapped within the gel. When placed in monolayer culture, rabbit and human chondrocytes, and Swarm rat chondrosarcoma cells attach, flatten, spread, and dedifferentiate by beginning to synthesize type I collagen and small non-aggregating proteoglycans. Matrix macromolecules produced in monolayer culture diffuse out into the medium and are not retained to form an intact matrix. (Although cell phenotype may be maintained in monolayer culture for bovine chondrocytes, a rounded cell shape is not [18].) Cell shape has been implicated as the primary determinant of the phenotype and recent studies [19, 20] have suggested that the integrity of the microfilament cytoskeletal structure may be more proximal to phenotypic change than is cell shape.

Agarose culture of chondrocytes has been used as an *in vitro* model for studying matrix degradation (induced by retinol) which may resemble that which occurs *in vivo* in early stages of osteoarthritis. Possible therapeutic agents such as anti-invasion factor, Arteparon, Eglin C, and pepstatin (most are primarily protease inhibitors) have been tested [12]. The ability to selectively seed certain cell populations has allowed the study of differences between cell subpopulations. Cells from the superficial zone (top 20-40 μm) of bovine metacarpal phalangeal cartilage were shown to have a more irregular shape, to divide slower, to synthesize and retain less proteoglycan, to synthesize a smaller and less aggregable proteoglycan, and to produce larger collagen

fibrils, than chondrocytes from deeper zones [13, 14]. Transparency of the agarose system has allowed the study of cell size over the culture period [17] and the study of colony formation in response to insulin-like growth factor-I and growth hormone [21]. Monolayer culture has been used to amplify cell number prior to placement in agarose and subsequent phenotype reexpression [16].

To date, most studies have used cell densities 10–100 times less than that found in native cartilage. Although the synthesis and accumulation of normal matrix components has been observed biochemically, no attempt has been made to measure the mechanical, electromechanical, and physicochemical properties of the matrix. Nevertheless, these studies suggest that the agarose/chondrocyte system may be ideally suited for examining the synthesis of a mechanically functional cartilage-like matrix.

The agarose/chondrocyte system may also benefit the examination of transduction mechanisms which mediate cell response to mechanical and electrical stimuli to the tissue. The amount of matrix present during stimulation may be controlled by choosing different time points during culture. For example, the choice of an early time point will highlight cell compression and reduce physicochemical and direct cell-matrix interactions. Transparency of the system may allow measurements of single cell properties such as cell shape or those exhibited by fluorescent probes. And lastly, the capacity to control the population of cells in a given experiment will have numerous applications.

Continuum Models of the Physical Properties of Cartilage Matrix

The physical properties of cartilage, that is its large compressive stiffness, the existence of electrokinetic phenomena and electrostatically influenced internal swelling pressures and ion distributions, can be thought of as resulting from a highly charged proteoglycan gel enmeshed within a collagen framework. The PG, containing a large number of fixed charge groups which repel each other, has a tendency to swell in the native state but is contained by tensile stress within the collagen fibril network. Although the collagen is vital in not only containing the PG's but in resisting tensile

and shear strain, it is the PG that is the determinant of many properties related to compressive stress. In the physiologic state, electrostatic repulsion between fixed charge groups contributes about one-half of the equilibrium modulus [22]. Transport properties such as hydraulic permeability, electrical conductivity, and electrokinetic coefficients, are also significantly affected by interactions within the proteoglycan component of the matrix [23, 24].

Macrocontinuum Theories

Most theories pertaining to the mechanical, electromechanical, and physico-chemical properties of cartilage matrix, and other charged, porous materials, have been macrocontinuum theories. Such theories inherently ignore molecular structure by averaging over a volume element large enough to contain many molecular components. The characteristic dimension is then much larger than the Debye length ($\sim 8\text{\AA}$ in physiological saline) so that quasineutrality is assumed valid everywhere except over a small region at the tissue-liquid interface [5].

Equilibrium properties, such as ionic distributions and osmotic swelling pressure, are characterized by Donnan equilibrium in which a spatially invariant electrostatic potential exists (due to fixed charge) in the tissue and is different from that in the bath [25]. The exponential nature of the Boltzmann distribution demands that more counterions are attracted than cations are repelled resulting in a higher total ionic concentration in the tissue than in the bath. The excess ionic concentration is interpreted as a Donnan osmotic swelling pressure using van't Hoff's relation. Mathematically the model is very simple, being two algebraic relations requiring knowledge of bath ionic strength, the fixed charge density, and mean ionic activity coefficients both in the tissue and in the bath. The disadvantage is that equilibrium measurements of the activity coefficient in the tissue requires the assumption of Donnan theory so that the validity of the theory itself is not determined [26, 27, 28, 29]. Some attempts have been made to derive expressions for the activity coefficients based on molecular structure using polyelectrolyte condensation theory [30, 31]. These attempts have

met with limited success and are excursions into a microcontinuum description.

Microcontinuum Theories

The effort in the microcontinuum approach is to relate properties to molecular structure. Judicious choice of the molecular model is important in order to obtain a solvable set of equations that still captures the elements of molecular structure that give rise to particular properties. Given the predominance of the proteoglycan as the main contributor to osmotic swelling pressure, ion distribution, and transport properties, the choice to be made is one of geometry.

The basic molecular unit of the PG is the chondroitin sulfate (a glycosaminoglycan or GAG) disaccharide chain. Each disaccharide contains two charges, a carboxyl and a sulfate, both ionized at physiological pH. Perhaps 50 chains of about 40 disaccharides each are covalently linked to a core protein forming a brush-like proteoglycan monomer of $\sim 10^6$ MW which is secreted by the cell as a unit. To contribute functionally to tissue properties, the monomer must find a hyaluronic acid chain to which a noncovalent bond is then formed, being stabilized by a link protein, to form a proteoglycan aggregate [32]. The proteoglycan is then effectively trapped within the collagen network and can not diffuse out of the tissue. A geometrical model of an aggregate, a monomer or even a finite length chondroitin sulfate chain would produce considerable mathematical difficulties in solving the relevant Poisson-Boltzmann equation. The highest level of tractable complexity is that of a rod-like polyelectrolyte, representing a cross section of a chondroitin sulfate (CS) chain.

The CS chain is of the correct length scale when considering properties arising from electrostatic repulsion. Electrostatic forces between charged bodies in an isotonic electrolyte solution in equilibrium are completely shielded across distances greater than a few nanometers (CS diameter ~ 1 nm). If the rod is considered to be a monomer, with a diameter of ~ 100 nm, any reasonable degree of hydration would place monomers far enough apart to shield any electrostatic interactions. This is not the case in the tissue. Electron microscopy of intact tissue has indicated that PG

monomers are packed so tightly that a CS chain on one monomer may be as close to a CS chain on another monomer as it is to an adjacent chain on the same monomer [33].

The microscopic picture is then a meshwork of CS chains stabilized in place by the hierarchy of monomer (core protein), aggregate (hyaluronic acid), and collagen interactions. There may be some non-random orientation of the meshwork giving rise to periodic arrays or nematic phases [34], at least within limited domains. However, as a first approach, the assumption of an isotropic phase is accompanied by sufficient complexity. The model is then the cell-model where a charged rod of infinite extent is surrounded by an annulus of electrolyte. The ratio of the two radii is determined by polyelectrolyte concentration, or equivalently by tissue hydration.

CHONDROCYTES IN AGAROSE

Summary

We have studied the ability of cartilage cells extracted from native cartilage to synthesize and accumulate a normal, cartilage-like extracellular matrix in agarose gel culture. We have characterized the extent and the time evolution of chondrocyte proliferation, synthesis of GAG and proteins, loss of GAG, and total deposition of GAG-containing matrix within agarose gels during long-term culture. To assess whether the matrix deposited within the agarose gel is a mechanically functional cartilage-like matrix, we measured several important mechanical and electromechanical properties of the agarose/chondrocyte disks at selected times during long-term culture: equilibrium elastic modulus, dynamic stiffness, and streaming potential induced by oscillatory mechanical compression. The results of these studies suggest that (1) both normal chondrocytes and Swarm rat chondrosarcoma cells in agarose culture can, under proper culture conditions, continue to synthesize matrix macromolecules at a rate similar to that in native cartilage, and (2) chondrocytes in agarose

can successfully mediate the assembly and accumulation of a normal, mechanically functional extracellular matrix.

Previous experiments of chondrocytes or chondrosarcoma cells cultured in agarose utilizing a cell density ranging from $(1 - 20) \times 10^6$ cells/ml and an agarose concentration in the range of $(1 - 5)\%$ cultured in serum supplemented Dulbecco's Modified Eagles Medium (DMEM) have identified an optimal system consisting of 20×10^6 cells/ml in 2% agarose. Two experiments using normal chondrocytes with these parameters have been completed yielding similar results. Experiments using Swarm rat chondrosarcoma cells have also been completed.

Methods

Articular cartilage from the femoropatellar groove from 1-to 2-week-old calves was harvested as previously described [35] and incubated in DMEM supplemented with 12.5 mM HEPES, 0.1 mM nonessential amino acids, 0.4 mM L-proline, 10% FBS, 50 μ g/ml ascorbate, and 0.1% penicillin/streptomycin changed daily at 5% CO₂, 37°C. One week later cells were extracted by sequential pronase and collagenase digestion [18]. In addition, Swarm rat chondrocytes were prepared for incorporation into agarose gels as previously described [17].

Chondrocytes were mixed into media containing 2% (w:v) low melting temperature (FMC) SeaPlaque agarose [12, 17] at $\sim 2 \times 10^7$ cells/ml and cast at 37°C between slab gel electrophoresis plates separated by 1-mm-thick Teflon spacers, as shown schematically in Figure 1. After gelling at 4°C for 2 h, 16-mm-diameter by 1-mm-thick disks were cored from the gel. The chondrocyte/agarose disks were subsequently cultured on top of nylon mesh (to promote nutrient diffusion from below). Media (as above) was changed daily and analyzed for GAG content by dimethyl-methylene blue (DMB) dye binding [36]. Control disks without chondrocytes were prepared and maintained in the same manner.

The mechanical and electromechanical properties of chondrocyte/agarose disks and control disks were measured in uniaxial confined compression using the test cham-

Preparation of Chondrocyte/Agarose Plugs ~2 Days

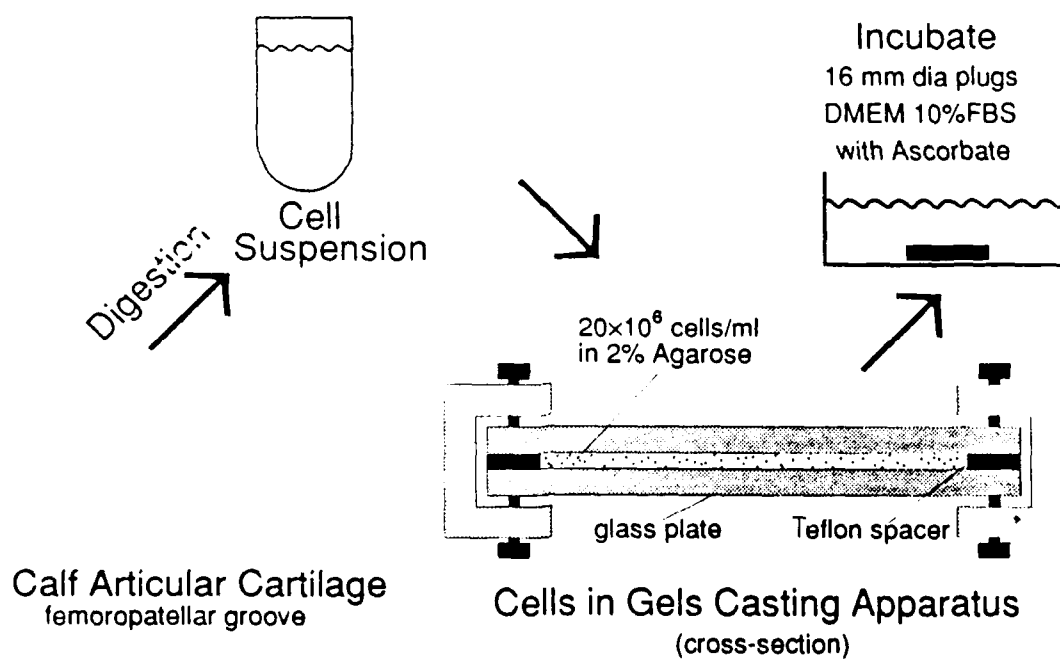
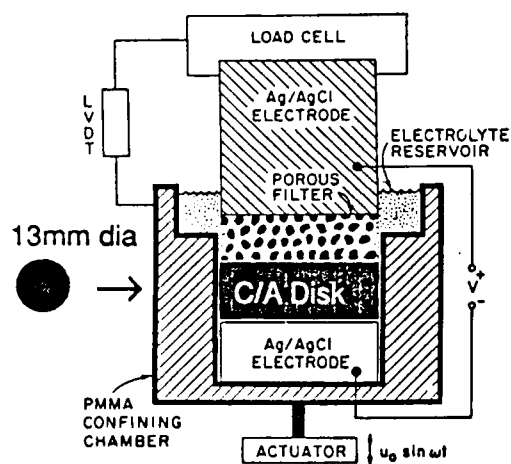


Figure 1. Preparation of chondrocyte/agarose cultures.

Mechanical and Electromechanical Testing



Biochemical Analysis

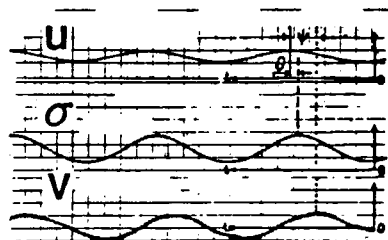
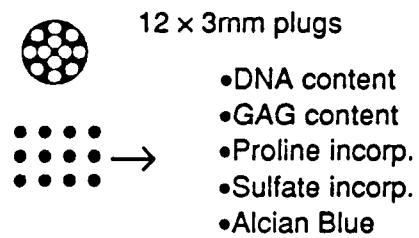


Figure 2. Mechanical, electromechanical and biochemical tests.

has been schematically in Figure 2, which was mounted in a Dynastat mechanical tester. Several 13-mm diameter disks were cored from the larger disks removed from culture at selected intervals, and placed between silver/silver chloride electrodes separated by a porous platen, all bathed in phosphate-buffered saline (PBS) (Fig. 2) [37]. A 20% static offset strain was applied and the load recorded until stress relaxation reached equilibrium. This equilibrium load and strain was used to compute the equilibrium elastic confined compression modulus. A 0.5% sinusoidal strain was then superimposed at frequencies between 0.01 and 1 Hz, and the resulting oscillatory load and streaming potential were recorded. Disks were then removed, weighed, lyophilized, and frozen and reweighed. The hydraulic permeability, electrokinetic coefficient, oscillatory stiffness, and streaming potential were computed from the data as described previously [37, 23].

Each week, groups of 9 to 12 3-mm-diameter disks were separately incubated for 16 h in media containing 10 $\mu\text{Ci/ml}$ [^{35}S]sulfate and 20 $\mu\text{Ci/ml}$ [5- ^3H]proline to assess GAG and protein synthesis, respectively (Fig. 2). These disks were washed in DMEM and digested with papain. Radiolabel incorporation was assessed by scintillation counting, and GAG was assessed by the DMB dye binding assay. In addition, the content of deoxyribonucleic acid (DNA) was measured in these same specimens by means of a fluorescence enhancement assay using the Hoechst 33258 dye [38].

Results and Discussion

Normal Chondrocytes

Table 1 shows the biochemical properties of agarose/chondrocyte disks on day 50 of a long-term culture that was maintained for 70 days. These properties are compared to those of intact calf articular cartilage similar in age and location to that from which the cells were extracted. In agarose/chondrocyte disks, total GAG content increased 7-fold over 10 weeks in agarose culture (Fig. 3) reaching $\sim 25\%$ of that in native parent cartilage disks (Table 1). By day 30, the amount of GAG alone was approximately the same as the agarose content of agarose/chondrocyte disks.

Table 1. CHONDROCYTES IN AGAROSE : BIOCHEMICAL PROPERTIES ON DAY 50

COMPARISON : CHONDROCYTE/AGAROSE DISKS
and CALF CARTILAGE EXPLANTS

	Chondrocyte/ Agarose disk†	Calf Cartilage 'parent disks'
Total DNA ($\mu\text{g}/\mu\text{l}$ disk vol.)	0.14 ± 0.02 (12)	0.56 ± 0.13 (30) [1]
Cell Density (10^6 cell/ml) (7.7pg/cell[7])	20.2 ± 2.8 (12)	73 ± 17 (30) [1]
Total GAG ($\mu\text{g}/\mu\text{l}$ disk vol.)	14.1 ± 2.6 (12)	57 ± 11 (30) [1]
GAG release rate ($\mu\text{g}/(\mu\text{l}$ disk vol)/day)	0.20 ± 0.03 (12)	0.62 ± 0.12 (12) [2]
GAG accumulation rate ($\mu\text{g}/(\mu\text{l}$ disk vol)/day)	0.22 ± 0.03 (12)	1.65 [1]
Sulf-incorp. (nmol sulfate/ 10^6 cell/day)	22 ± 4 (12)	45 ± 21 (20) [1]
Prol-incorp. (nmol proline/ 10^6 cell/day)	17 ± 2 (12)	20.1 ± 9.5 (28) [1]

† data for day 50

MEAN \pm SD (n)

1) Sah RL et al. *J Orthop Res*, 7:619, 1989.

2) Sah RL et al. *Trans ORS*, 14:50, 1989.

DNA content appeared to increase by a factor of 2 over the 10-week period (Fig. 3). The significant increase in disk wet weight and thickness (Fig. 4) with time in culture is a direct consequence of the accumulation of matrix and the high osmotic swelling pressure of the GAG constituents.

Sulfate and proline incorporation (Fig. 5) reflects the rate of synthesis of proteoglycans and total protein, respectively. Sulfate and proline incorporation levels in agarose culture (Fig. 5) were similar to that in the intact parent cartilage (Table 1). The decrease in radiolabel incorporation after day 24 is consistent with the possibility that gradual accumulation of matrix down-regulates matrix biosynthesis. While biosynthetic rates were similar for chondrocytes in agarose and cartilage, the GAG accumulation rate per disk volume in agarose (Table 1), calculated by linear regression of GAG content over the 10-week period (Fig. 5), was lower than that in intact cartilage. The rate at which GAG was released from the agarose disks was also lower (Table 1). These results are consistent with the fact that the cell density in the agarose disks is still 4-5 times lower than that in the parent cartilage tissue.

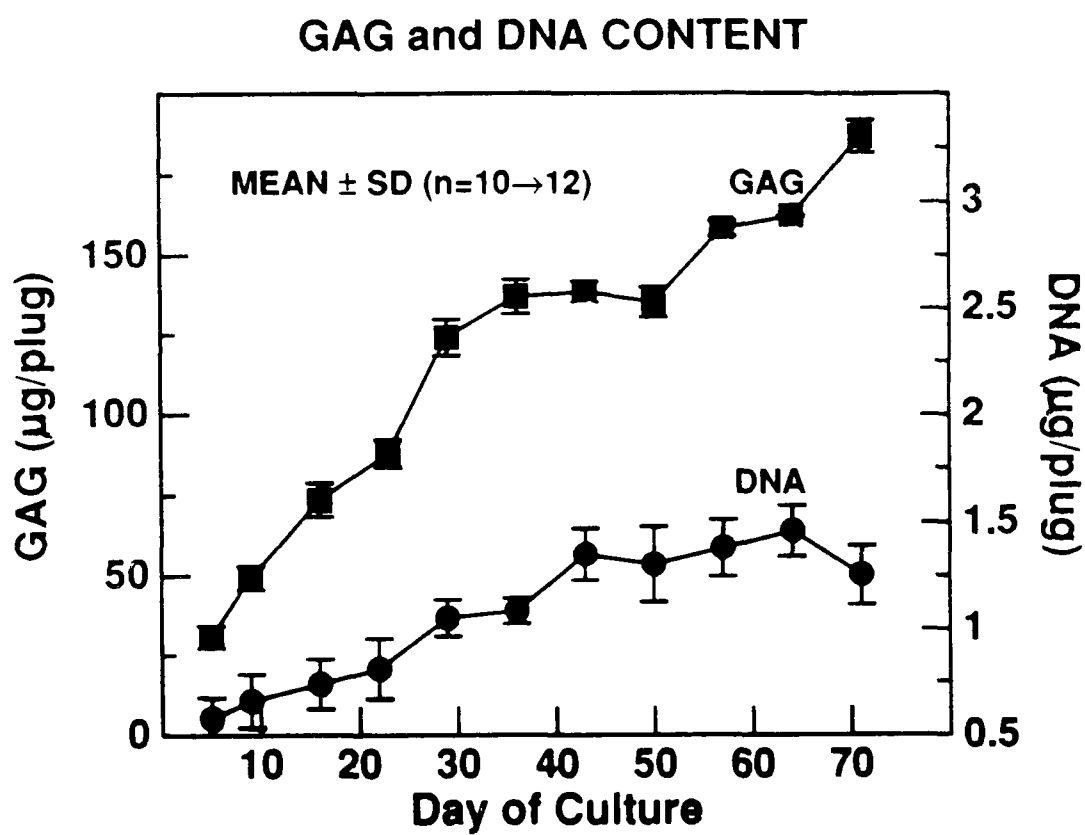


Figure 3. Chondrocytes in agarose : GAG and DNA content during culture.

NORMALIZED WET WEIGHT and THICKNESS

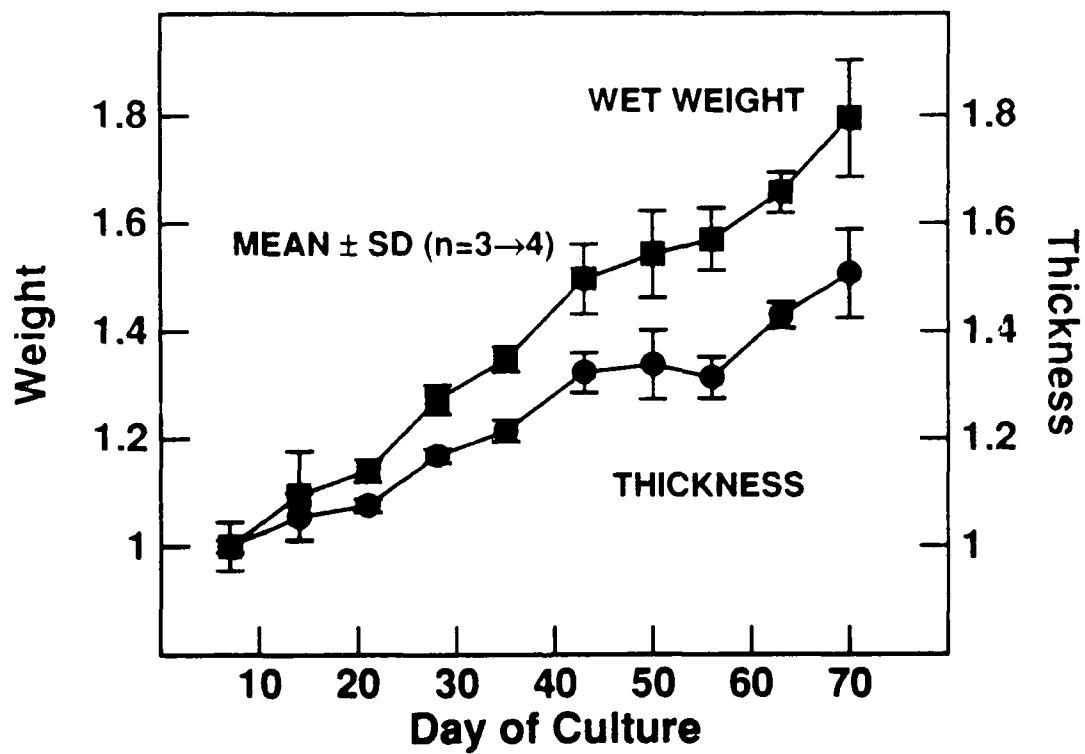


Figure 4. Chondrocytes in agarose : geometrical properties during culture.

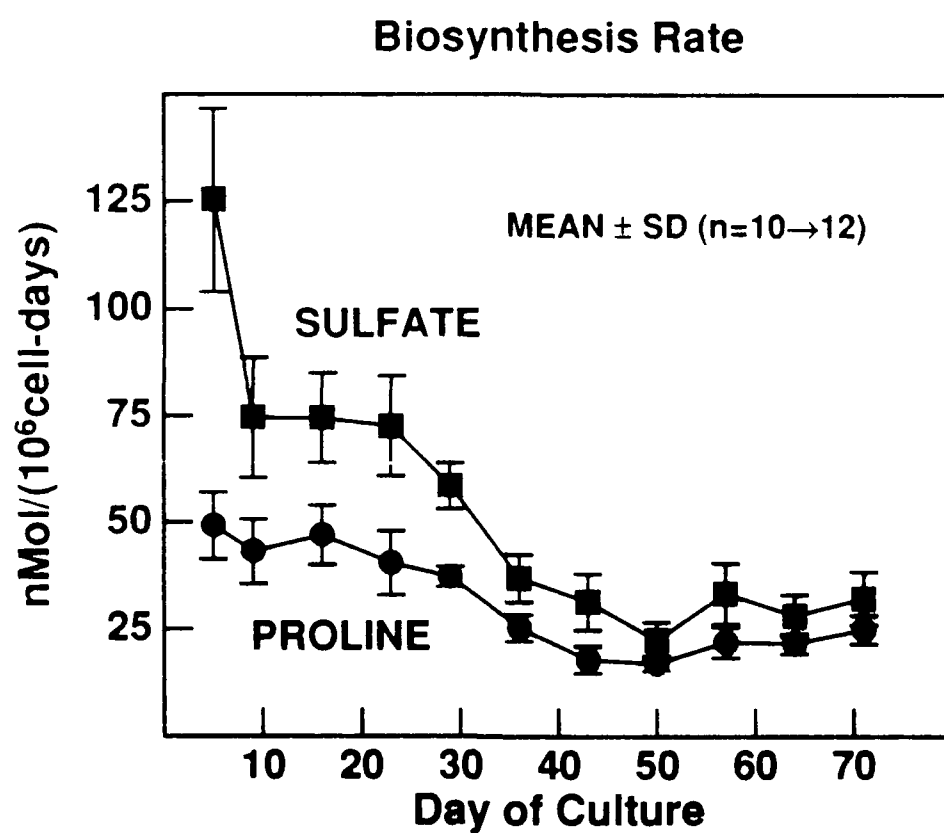


Figure 5. Chondrocytes in agarose : radiolabel incorporation during culture.

Cell-laden disks showed significantly enhanced equilibrium modulus, dynamic stiffness, and streaming potential with increasing time in culture compared to controls (Figs. 6 and 7), consistent with the increased GAG content found in the same specimens. The existence of the streaming potential and the increase in the potential with time in culture is especially significant, since this streaming potential gives a nondestructive measure of the quality of the newly synthesized extracellular matrix secreted and assembled by the cells. If the newly synthesized proteoglycans had not been functionally immobilized within the developing matrix (as occurs in intact cartilage), there would have been little or no increase in streaming potential (Fig. 7).

The frequency response of the streaming potential and dynamic stiffness is also an important measure of the functional behavior of the extracellular matrix. The dynamic stiffness and streaming potential of agarose/chondrocyte disks increased with frequency (Fig. 8) in a manner characteristic of the poroelastic behavior of cartilage [37, 23]. Sinusoidal stress-strain and streaming potential were essentially linear in the 0.01-1 Hz range (total harmonic distortion < 8%). The frequency dependence of the dynamic stiffness and streaming potential amplitude of a disk of normal cartilage is also shown in Fig. 8 for comparison. The increase in streaming potential amplitude with increasing frequency is due to the increase in relative fluid velocity produced at higher compression rates. This relative fluid velocity is responsible for producing the streaming potential.

The equilibrium modulus and the computed hydraulic permeability of agarose/chondrocyte disks at day 50 are compared to values for parent calf cartilage disks in Table 1. The permeability is slightly higher, consistent with the larger pore size and lower GAG content of the chondrocyte/agarose disk compared to cartilage.

Swarm Rat Chondrosarcoma Cells

In another set of experiments, Swarm rat chondrosarcoma cells were incorporated into 2% agarose gels as before. During 4 weeks in culture, the total GAG

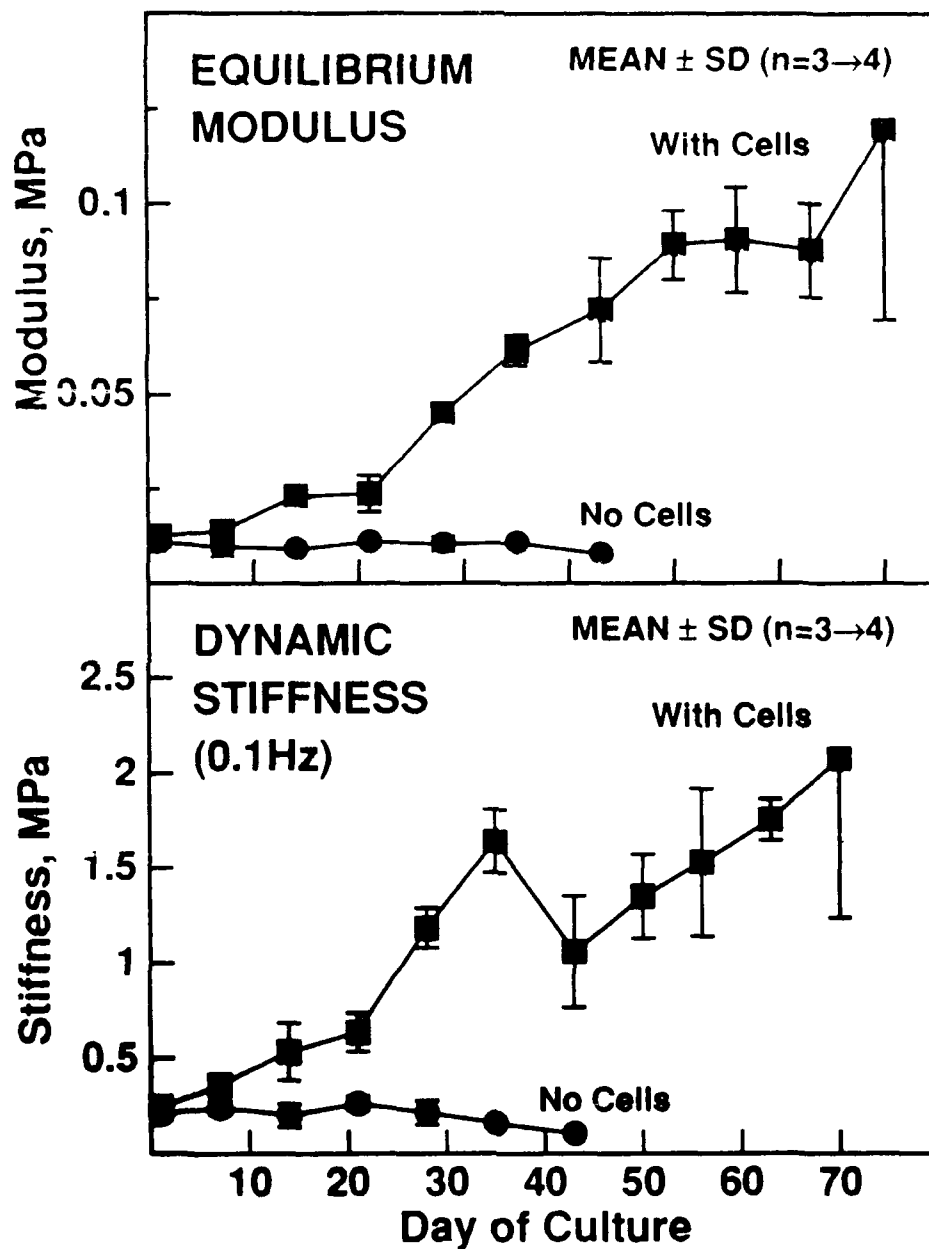


Figure 6. Chondrocytes in agarose : stiffness during culture.

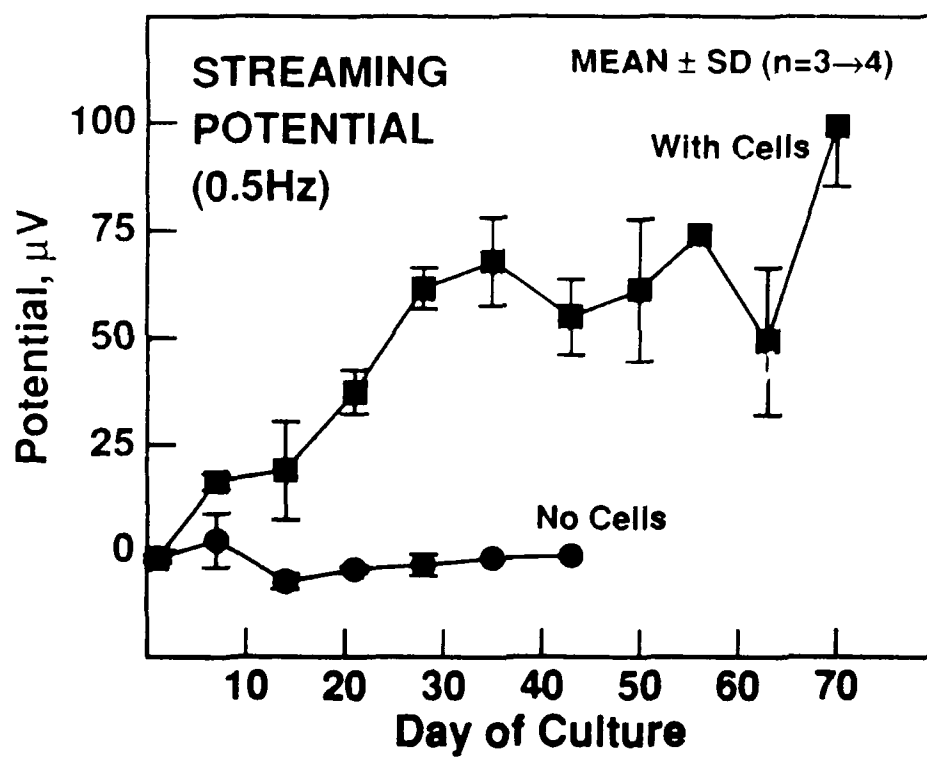


Figure 7. Chondrocytes in agarose : streaming potential during culture.

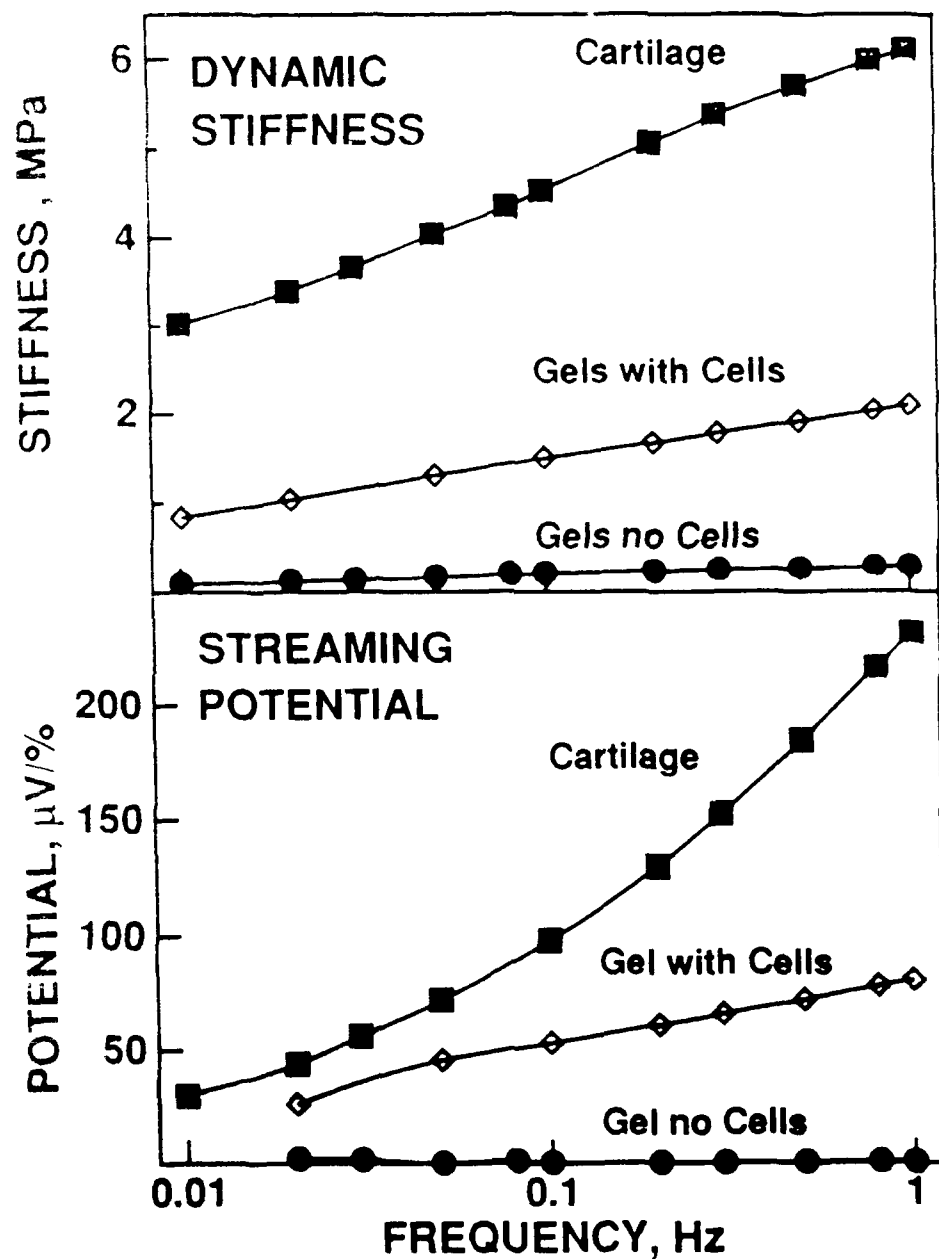


Figure 8. Chondrocytes in agarose : stiffness and streaming potential of chondrocyte/agarose plugs displays poroelastic behavior like articular cartilage.

Table 2. CHONDROCYTES IN AGAROSE : PHYSICAL PROPERTIES ON DAY 50.

**COMPARISON : CHONDROCYTE/AGAROSE DISKS
and CALF CARTILAGE EXPLANTS**

	Chondrocyte/ Agarose disk†	Calf Cartilage 'parent disks'
Equilibrium Modulus (kPa)	91 ± 7 (3)	470 [1,2]
Dynamic Stiffness (0.5Hz) (MPa)	1.64 ± 0.31 (3)	4.7 [1,2]
Streaming Potential (0.5Hz) (μV/%)	61 ± 17 (3)	150-600 [1,2]
Hydraulic Perm. (m ⁴ /N·s × 10 ¹⁵)	5.1 ± 1.9 (3)	3.5 [1,2]
Electrokinetic Coefficient (mV/MPa)	3.7 ± .8 (3)	20 [1,2]

† data for day 50

MEAN ± SD (n)

1) Frank EH & Grodzinsky AJ. *J Biomech*, 20:629, 1987.

2) Hey LA *BS Thesis*, MIT, 1984.

content within the agarose/chondrocyte disks increased almost 20 fold, while DNA content increased by 2-3 fold (data not shown). After 4 weeks, dynamic stiffness and streaming potential of cell-laden disks had also increased above control levels. These experiments were actually performed before those involving normal calf chondrocytes. Because of changes and improvements in the methodology in mixing and casting the gels, it is difficult to compare the absolute value of changes observed with normal chondrocytes and chondrosarcoma cells thus far. It is clear, however, that definitive changes have been observed with both types of cells.

Conclusions

The results of these studies suggest that: (1) both normal chondrocytes and Swarm rat chondrosarcoma cells in agarose culture can, under proper culture conditions, continue to synthesize matrix macromolecules at a rate similar to that in native cartilage, and (2) chondrocytes in agarose can successfully mediate the assembly and accumulation of a normal, mechanically functional extracellular matrix. These results provide support for the long-term objectives of this research in that

the chondrocyte/agarose system appears to be an appropriate model with which to study the mechanisms by which physical forces (e.g., electrical and mechanical) may interact with mammalian cells. The chondrocytes can be maintained in a natural environment which, in certain ways, is more amenable than that of intact cartilage to the study of mechanism at the single cell level.

MODEL OF EQUILIBRIUM PROPERTIES

Summary

A microcontinuum model based on the unit-cell model of rod-like polyelectrolytes, and representing a chondroitin sulfate molecule, is used to predict osmotic swelling pressures in proteoglycan solutions and the ionic strength dependent component of the equilibrium modulus of articular cartilage. The model predictions are compared to Donnan theory for proteoglycan solutions. Donnan theory predicts higher pressures and is inconsistent with the rod-model prediction. Donnan theory may be made to fit experimental data by ad-hoc usage of activity coefficients and unphysical designation of excluded volume pressure. The rod-model only requires knowledge of nonthermodynamic, structural parameters which may be measured independently of the theory. The rod-model accurately describes the osmotic pressure of proteoglycan solutions and the ionic strength dependent component of the equilibrium modulus of articular cartilage with parameters which are reasonable when compared to those of chemical-structural models of chondroitin sulfate, or those obtained from other experiments.

Introduction

The model considered here is the microcontinuum *unit cell* [39, 40, 41] where the solid is represented as a circular cylinder with a uniform surface charge and the electrolyte fluid surrounds the solid out to a fictitious cylindrical boundary, the radius of which is determined by the solid to fluid volume ratio (Fig. 9). The osmotic swelling

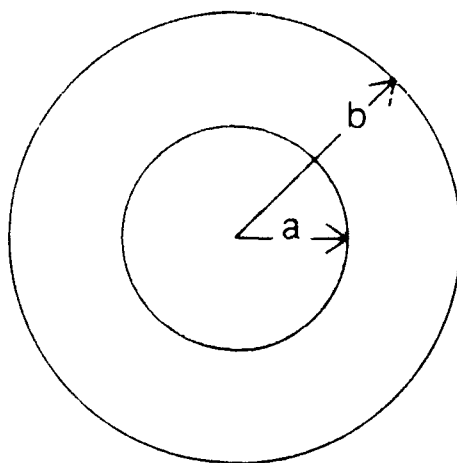


Figure 9. Unit Cell.

pressure and ion distributions will be calculated using the Poisson-Boltzmann (PB) equation. The PB equation is an approximation to the exact many body problem [42]. In the PB approximation the solvent is treated as an incompressible dielectric continuum and the potential of mean force on an ion is equated with the electrostatic potential. The PB equation excludes effects such as dielectric saturation and electrostriction while the more exact model includes ionic polarizability, short-range interionic repulsion, and any other 2-particle correlations beyond the mean field, point ion approximation. However, many theoretical and experimental studies have confirmed the accuracy of the PB equation in a variety of situations [43].

Comparison to Monte Carlo simulations where the electrolyte model the simple primitive model (incorporates hard sphere ion-ion repulsion) have suggested that the PB approximation is valid when the concentration of divalent ions is low [41, 44]. Divalent ions have more significant 2-particle correlations which push them closer to the charged surface than is predicted by the PB equation, reducing the osmotic pressure. Experiments measuring surface potentials and forces between charged surfaces have agreed well with PB theory [43].

Condensation theory, another approach to the properties of polyelectrolytes, has been formulated using empirical rules by Manning [30] and Oosawa [45]. It has been shown to be a special case of the PB formulation and need not be used since the PB equation is not difficult to solve numerically and the PB approximation is more general in consequence than Condensation theory [46, 47].

Numerical Solution of the Poisson-Boltzmann Equation

The electrostatic potential $\tilde{\phi}$ and charge density $\tilde{\rho}$ satisfy Poisson's equation

$$\nabla^2 \tilde{\phi} = \frac{-\tilde{\rho}}{\epsilon} \quad (1)$$

with the medium permittivity ϵ . The $\tilde{\phi}$ represents a dimensional (unnormalized) quantity. The charge in the fluid is mainly due to dissociated sodium chloride (NaCl) and is thus represented as satisfying the Boltzmann distribution for a monovalent electrolyte.

$$\begin{aligned} \tilde{\rho} &= F(\tilde{C}_+ - \tilde{C}_-) \\ &= FC_0(e^{\frac{-F\tilde{\phi}}{RT}} - e^{\frac{+F\tilde{\phi}}{RT}}) \\ &= -2FC_0 \sinh\left(\frac{F\tilde{\phi}}{RT}\right) \end{aligned} \quad (2)$$

where F is the faraday constant, R the gas constant, T temperature, and C_0 the concentration of NaCl in the bath where $\tilde{\phi}$ is set to zero. The PB equation is then obtained.

$$\nabla^2 \tilde{\phi} = \frac{2FC_0}{\epsilon} \sinh\left(\frac{F\tilde{\phi}}{RT}\right) \quad (3)$$

The boundary condition on the solid cylinder surface ($\tilde{r} = \tilde{a}$) arising from Gauss's law is

$$\tilde{\sigma} = \epsilon_{a+} \tilde{E}_{r,a+} - \epsilon_{a-} \tilde{E}_{r,a-} \quad (4)$$

where $\tilde{\sigma}$ is the uniform surface charge, \tilde{E}_r is the radial component of the electric field, $a+$ indicates just outside the cylinder, and $a-$ just inside. Inside the cylinder the field

is laplacian, and is given by

$$\bar{\phi}_{in} = A + \sum_{n=1}^{\infty} (B_n \bar{r}^n \cos n\theta + C_n \bar{r}^n \sin n\theta). \quad (5)$$

Due to the azimuthal symmetry, all B's and C's are zero so that there is no field inside. Then,

$$\bar{\sigma} = \epsilon_{a+} \bar{E}_{r,a+} \quad (6)$$

$$= -\epsilon \left. \frac{d\bar{\phi}}{d\bar{r}} \right|_{\bar{a}}. \quad (7)$$

At the outer cell boundary ($\bar{r} = \bar{b}$),

$$\left. \frac{d\bar{\phi}}{d\bar{r}} \right|_{\bar{b}} = 0 \quad (3)$$

is required by considering two unit cells butted together (without equation (8) there would be a sheet of charge surrounding each unit cell). With the normalization

$$\phi = \frac{F\bar{\phi}}{RT} \quad (9)$$

$$r = \frac{\bar{r}}{\delta} \quad (10)$$

$$\sigma = \frac{\bar{\sigma}}{\sigma_0} \quad (11)$$

where

$$\delta^2 = \frac{RT\epsilon}{2C_0 F^2} \quad (12)$$

$$\sigma_0 = \frac{\epsilon RT}{\delta F} \quad (13)$$

and where δ is the debye length, equations (3), (7), and (8) become

$$\frac{d^2\phi}{dr^2} + \frac{1}{r} \frac{d\phi}{dr} = \sinh(\phi) \quad (14)$$

$$\left. \frac{d\phi}{dr} \right|_a = -\sigma \quad (15)$$

$$\left. \frac{d\phi}{dr} \right|_b = 0 \quad (16)$$

There is no known general analytic solution to equation (14) [48] and numerical solutions (Runge-Kutta) can be nonconvergent in the nonlinear regime, even with very small steps [49].

An efficient numerical solution can be formulated by solving equation (14) in intervals where the change in $\phi \ll 1$. Considering an interval (r_0, r_1) , equation (14) is linearized to

$$\psi = \phi - \phi_0 \quad (17)$$

where $\phi_0 = \phi(r_0)$. Then,

$$\sinh(\phi) = \sinh(\psi) \cosh(\phi_0) + \cosh(\psi) \sinh(\phi_0) \quad (18)$$

$$\cong \psi \cosh(\phi_0) + \sinh(\phi_0) \quad (19)$$

and equation (14) becomes

$$\frac{d^2\psi}{dr^2} + \frac{1}{r} \frac{d\psi}{dr} - \psi \cosh(\phi_0) = \sinh(\phi_0) \quad (20)$$

with the solution

$$\psi = C_1 I_0(\alpha r) + C_2 K_0(\alpha r) - \tanh(\phi_0) \quad (21)$$

and derivative

$$\frac{d\psi}{dr} = \alpha C_1 I_1(\alpha r) - \alpha C_2 K_1(\alpha r) \quad (22)$$

where I_n and K_n are modified Bessel functions of order n , and

$$\alpha^2 = \cosh(\phi_0). \quad (23)$$

C_1 and C_2 can be found with knowledge of ϕ_0 and ϕ'_0 . So that at r_0 ,

$$\psi(r_0) = 0 \quad (24)$$

$$\frac{d\psi(r_0)}{dr} = \phi'_0 \quad (25)$$

become

$$C_1 I_0(\alpha r_0) + C_2 K_0(\alpha r_0) = \tanh(\phi_0) \quad (26)$$

$$C_1 I_1(\alpha r_0) - C_2 K_1(\alpha r_0) = \frac{\phi'_0}{\alpha} \quad (27)$$

which, solved for C_1 and C_2 is

$$C_1 = \frac{\frac{\phi'_0}{\alpha} + \frac{K_1(\alpha r_0) \tanh(\phi_0)}{K_0(\alpha r_0)}}{I_1(\alpha r_0) + \frac{K_1(\alpha r_0) I_0(\alpha r_0)}{K_0(\alpha r_0)}} \quad (28)$$

$$C_2 = \frac{\tanh(\phi_0) - C_1 I_0(\alpha r_0)}{K_0(\alpha r_0)} \quad (29)$$

A step is taken to the new point r_1 by calculating $\psi(r_1)$ and $\psi(r_1)'$ from equations (21) and (22), which then serves as the starting point r_0 for the next step, with a restriction on the nonlinearity (second order term in (19)),

$$\frac{\psi^2(r_1)}{2} < \vartheta. \quad (30)$$

If the trial step violates equation (30), the step size is reduced until equation (30) is satisfied. The complete integration begins at the outer boundary ($r=b$) where (16) specifies $\phi'_0 = 0$ and a guess is taken for $\phi_0 = \phi(b)$. Equation (15) is satisfied by repeating the integration with different values of this initial $\phi(b)$ determined by polynomial interpolation of the pairs $(\phi(b), \frac{d\phi}{dr}|_a)$ until $\frac{d\phi}{dr}|_a = -\sigma$ to within a specified accuracy ($\sim 10^{-6}$). By using a five point discrete differentiation formula to calculate

the error in the solution to equation (14),

$$\text{error} = \frac{\frac{d^2\phi}{dr^2} + \frac{1}{r}\frac{d\phi}{dr} - \sinh(\phi)}{\sinh(\phi)}, \quad (31)$$

the error was found to be of the same order as ϑ which was chosen to be 10^{-6} .

Electrostatic Swelling Pressure in the Unit Cell

It is proposed that the swelling pressure due to the electrostatic repulsion of an array of charged rods is the pressure (osmotic) at the cell boundary minus that in the bath,

$$\tilde{P}_{\text{swell}} = RT(\tilde{c}_+(\tilde{b}) + \tilde{c}_-(\tilde{b}) - 2C_0) \quad (32)$$

$$= 2RTC_0(\cosh(\phi(\tilde{b}) - 1)) \quad (33)$$

This result has been shown by differentiating the free energy (comprised of the electrostatic energy of all the charge in the unit cell and the entropy of mixing of the mobile charge) with respect to a change in volume of the unit cell [40]. Here, the result of equation (33) will be found from the consideration of the fluid stress tensor in the unit cell with no reference to a cell free energy or hypothetical charging process. The two perspectives are complementary.

The thermodynamic definition of the molar chemical potential for species i [50],

$$\bar{\mu}_i = \bar{\mu}_i^0(T) + v_i\tilde{P} + RT \ln(\gamma_i x_i) + z_i F \tilde{\phi} \quad (34)$$

where $x_i = \frac{n_i}{\sum n_i}$ ($n_i = \#$ moles of species i) is the mole fraction, $v_i = \left. \frac{\partial V}{\partial n_i} \right|_{T, \tilde{P}, \tilde{\phi}, n_{j \neq i}}$ the partial molar volume, \tilde{P} the pressure of the mixture, γ_i the activity coefficient, z_i the valence, and $\tilde{\phi}$ the electrostatic potential. Neglecting temperature gradients and assuming ideality ($\gamma_i = 1$), the chemical potential of the uncharged solvent is,

$$\bar{\mu}_0 = v_0\tilde{P} + RT \ln x_0. \quad (35)$$

By definition,

$$1 = x_0 + x_+ + x_-, \quad (36)$$

and for dilute solutions,

$$x_+ + x_- \ll 1, \quad (37)$$

so that one gets

$$\ln x_0 \cong -(x_+ + x_-). \quad (38)$$

Then,

$$\tilde{\mu}_0 = v_0 \tilde{P} - RT(x_+ + x_-) \quad (39)$$

For small solutes (NaCl) the $v_i \tilde{P}$ term may be neglected [50],

$$\tilde{\mu}_+ = RT \ln x_+ + F \tilde{\phi} \quad (40)$$

$$\tilde{\mu}_- = RT \ln x_- - F \tilde{\phi}. \quad (41)$$

Each species is in equilibrium in the unit cell and between the cell and the bath (through the array of other rods) requiring,

$$\vec{\nabla} \tilde{\mu}_i = 0 \quad (42)$$

$$\tilde{\mu}_i = \text{constant} = 0 \quad (43)$$

since the constant is arbitrary. Then equation (39) defines the pressure,

$$\tilde{P} = \frac{RT(x_+ + x_-)}{v_0} \cong RT(\tilde{c}_+ + \tilde{c}_-) \quad (44)$$

The equilibrium force balance may be found from equations (40), (41), and (42),

$$0 = -\tilde{c}_+ \vec{\nabla} \tilde{\mu}_- - \tilde{c}_- \vec{\nabla} \tilde{\mu}_+ \quad (45)$$

$$= -RT \vec{\nabla}(x_+ + x_-) + F(x_+ - x_-)(-\vec{\nabla} \tilde{\phi}). \quad (46)$$

Dividing by v_0 ,

$$0 = -RT\vec{\nabla}(\tilde{c}_+ + \tilde{c}_-) + F(\tilde{c}_+ - \tilde{c}_-)(-\vec{\nabla}\tilde{\phi}). \quad (47)$$

Using equation (44) along with,

$$F(\tilde{c}_+ - \tilde{c}_-)(-\vec{\nabla}\tilde{\phi}) = \tilde{\rho}\vec{E} = \vec{\nabla} \cdot \vec{\overline{T}} \quad (48)$$

where $\vec{\overline{T}}$ is the electrostatic stress tensor,

$$\vec{\overline{T}} = \epsilon\vec{E}\vec{E} - \frac{\epsilon}{2}\vec{\overline{I}}E^2 \quad (49)$$

and $\vec{\overline{I}}$ the idemfactor, equation (47) becomes

$$0 = \vec{\nabla} \cdot (-\tilde{P}\vec{\overline{I}} + \vec{\overline{T}}), \quad (50)$$

which is the first integral of equation (3), the PB equation (multiply equation (3) by $\vec{\nabla}\tilde{\phi}$). The total stress tensor is then,

$$\vec{\overline{\Gamma}} = -\tilde{P}\vec{\overline{I}} + \vec{\overline{T}}. \quad (51)$$

The force on any volume may be found by,

$$\vec{F} = \oint_S \vec{\overline{\Gamma}} \cdot d\vec{S} \quad (52)$$

where S is the enclosing surface. There is no net force on the solid rod due to the azimuthal symmetry. This can be seen by constructing a volume enclosing the rod at its surface. In an actual array of cylindrical rods, only the central rod will possess this symmetry and experience no net force. For non-central rods there will be an asymmetry which will give rise to a net force on the rod (pushing it outwards) requiring a mechanical restraint (like the solid structure).

By forming a surface on the outer boundary of the unit cell where $\bar{T} = 0$ (due to equation (8)) it is seen that although no part of the unit cell experiences any net force, there is a pressure

$$\bar{P}_b = RT(\bar{c}_+(\bar{b}) + \bar{c}_-(\bar{b})) \quad (53)$$

$$= 2RTC_0 \cosh(\phi(\bar{b})) \quad (54)$$

which is higher than the pressure in the bath,

$$\bar{P}_0 = 2RTC_0. \quad (55)$$

And it is the difference,

$$\bar{P}_{swell} = \bar{P}_b - \bar{P}_0 = 2RT C_0 (\cosh(\phi(\bar{b})) - 1) \quad (56)$$

which constitutes the swelling pressure that is transmitted to the solid array by the previously mentioned asymmetries .

Comparison to Chondroitin Sulfate Solutions

The swelling pressure of chondroitin sulfate solutions has been measured by Urban et al. [27]. Commercially obtained CS preparations (purity $\sim 70\%$) were placed in a dialysis sac and equilibrated with a Polyethylene Glycol (PEG) solution of known osmotic pressure. Radioactive tracer ions were used to measure the fixed charge density (based on the Donnan model). The swelling pressure of the solution as a function of fixed charge density was then compared with that predicted by a *macroscopic ideal Donnan equilibrium* model at 2 ionic strengths, 0.15 M and 1.5 M. The expression for swelling pressure in the ideal Donnan model follows from bulk electroneutrality and ideal Donnan equilibrium,

$$\rho_m^- + C_+^D - C_-^D = 0 \quad (57)$$

$$C_+^D C_-^D = C_o^2 \quad (58)$$

where ρ_m is the macroscopic fixed charge in moles per litre tissue fluid, C_{\pm}^D are the Donnan ion concentrations in the polyelectrolyte phase and C_o is the concentration in the equilibrating bath. C_{\pm}^D are found from equations (57) and (58) ,

$$C_{\pm}^D = \mp \rho_m / 2 + \sqrt{\rho_m^2 / 4 + C_o^2} \quad (59)$$

from which the swelling pressure is taken as the osmotic pressure in the polyelectrolyte phase minus that in the bath,

$$P_{swell} = RT(C_+^D + C_-^D - 2C_o) \quad (60)$$

$$= RT(2\sqrt{\rho_m^2 / 4 + C_o^2} - C_o^2) \quad (61)$$

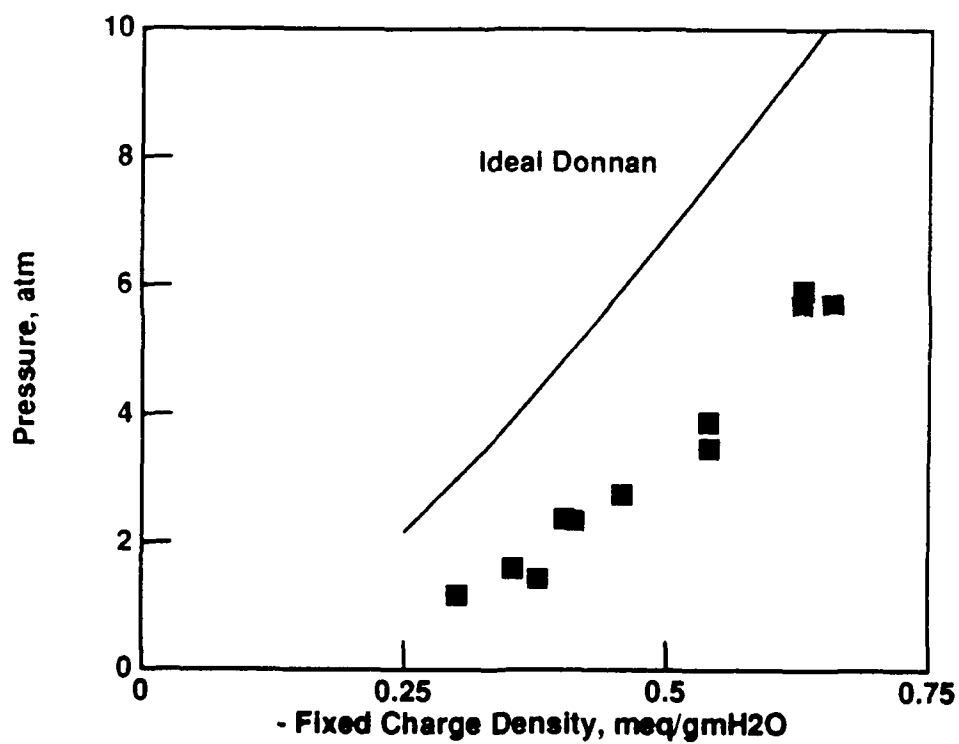
in units of kPa (101.325 kPa/atm). The data is shown along with the ideal Donnan prediction in Figures 10 and 11.

According to the macroscopic model, the discrepancy between model prediction and data in Figure 10 can be accounted for by introducing activity coefficients in an ad-hoc manner. Wells' modifications of Manning's expressions [27, 28] predict a swelling pressure much lower than that measured.

The underprediction of the ideal Donnan model in Figure 11 is suggested [27] to be due to excluded volume effects. However, at 1.5 M with a debye length of ~ 1.4 A, virtually no mean field, point ion, electrostatic contributions to swelling pressure will exist. Then the total swelling pressure in Figure 11 is interpreted to be due to excluded volume, and other forces not accounted for in the PB approximation; it is the difference in swelling pressure at 0.15 M and 1.5 M that is due to electrostatic repulsion and predicted by the unit cell model.

Figure 12 shows both data sets with polynomial best fits. The subtraction of the 2 curves at 4 points is plotted in Figure 13 along with a best fit micromodel

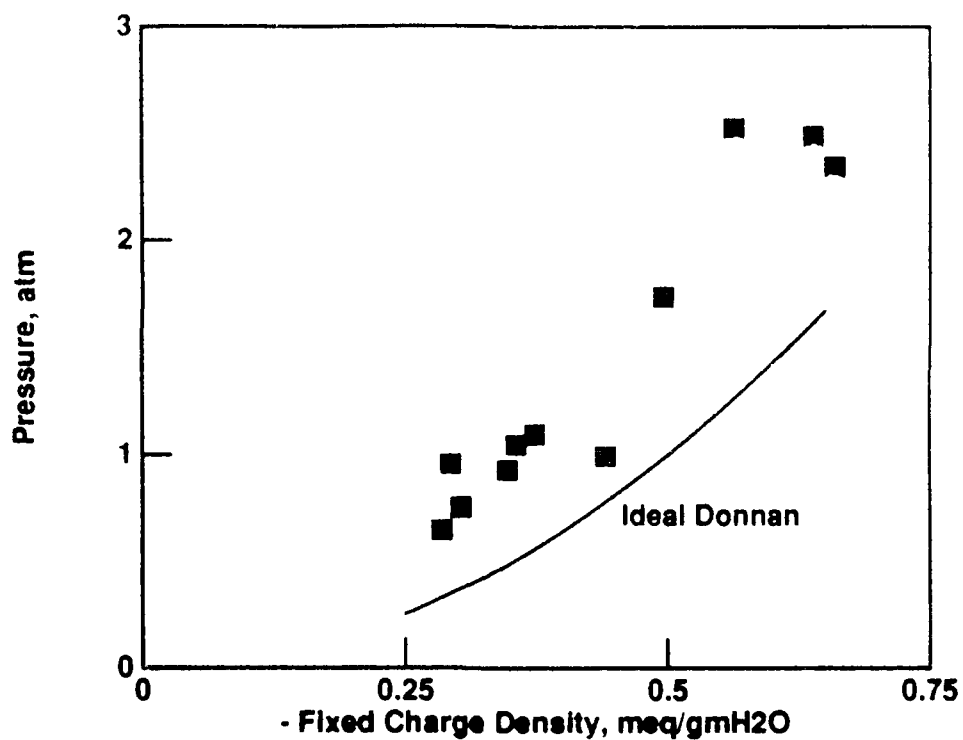
Swelling Pressure of CS vs.FCD at 0.15 M NaCl



Urban JPG Maroudas A Biorheology vol. 16 pg 457 fig 5, 1979

Figure 10. Swelling pressure of chondroitin sulfate solution in 0.15 M NaCl.

Swelling Pressure of CS vs.FCD
at 1.5 M NaCl



Urban JPG Maroudas A Biorheology vol. 16 pg 457 fig 6, 1979

Figure 11. Swelling pressure of chondroitin sulfate solution in 1.5 M NaCl.

Table 3. MICROMODEL FIT (on $\bar{\sigma}$) WITH $\bar{a} = 6$ A FIXED

$\bar{a} = 6 \text{ A}$		$\bar{\sigma} = -0.1379 \text{ C/m}^2$		
$chi = 0.04569$				
$\bar{\rho}_m$	\bar{b}	$(\bar{b} - \bar{a})$	model P	data P
0.35	22.92	16.92	0.6017	0.5744
0.45	20.41	14.41	1.283	1.159
0.55	18.64	12.64	2.189	2.086
0.65	17.31	11.31	3.276	3.414

prediction. The parameters required to solve equation (3) to obtain the swelling pressure are the radii \bar{a} , \bar{b} , the surface charge $\bar{\sigma}$, and the ionic strength C_o . The permittivity ϵ is that of water at 25°C,

$$\epsilon = 78.3\epsilon_o = 6.93 \times 10^{-10} \text{ Farad/m} \quad (62)$$

The unspecified parameters in the unit cell model are then \bar{a} , \bar{b} , and $\bar{\sigma}$, subject to the constraint,

$$\bar{\rho}_m = \frac{2\bar{\sigma}\bar{a}}{10^3 F(\bar{b}^2 - \bar{a}^2)}, \quad (63)$$

leaving 2 degrees of freedom. The variable parameters were chosen to be \bar{a} and $\bar{\sigma}$ so that \bar{b} is determined from equation (63). The model was then fit using a 2 dimensional minimization of the sum of the squares of the differences (χ) between data and model at 4 points on the $-\bar{\rho}_m$ axis. The data could be fit with more than one set of $(\bar{a}, \bar{\sigma})$, depending on the choice of starting point and end condition. By fixing the rod radius \bar{a} and performing a 1-dimensional minimization (on $\bar{\sigma}$), the 3 best fits in Tables 3, 4, 5 were found. It is the fit in Table 3 that is shown in Figure 13.

As there are no standard deviations on the data, confidence limits for the fits cannot be stated. It is most likely that none of the 3 shown actually better represents the data than the other two. Thus, apparently there is really only 1 degree of

Table 4. MICROMODEL FIT (on $\bar{\sigma}$) WITH $\bar{a} = 9$ A FIXED

$\bar{a} = 9 \text{ \AA}$	$\bar{\sigma} = -0.1156 \text{ C/m}^2$			
$chi = 0.02578$				
$\bar{\rho}_m$	\bar{b}	$(\bar{b} - \bar{a})$	model P	data P
0.35	26.42	17.42	0.5547	0.5744
0.45	23.68	14.68	1.238	1.159
0.55	21.76	12.76	2.171	2.086
0.65	20.33	11.33	3.303	3.414

Table 5. MICROMODEL FIT (on $\bar{\sigma}$) WITH $\bar{a} = 15$ A FIXED

$\bar{a} = 15 \text{ \AA}$		$\bar{\sigma} = -0.0977 \text{ C/m}^2$		
$chi = 0.01498$				
$\bar{\rho}_m$	\bar{b}	$(\bar{b} - \bar{a})$	model P	data P
0.35	33.06	18.06	0.5000	0.5744
0.45	30.00	15.00	1.188	1.159
0.55	27.88	13.88	2.159	2.086
0.65	26.31	11.31	3.357	3.414

Swelling Pressure of CS vs FCD

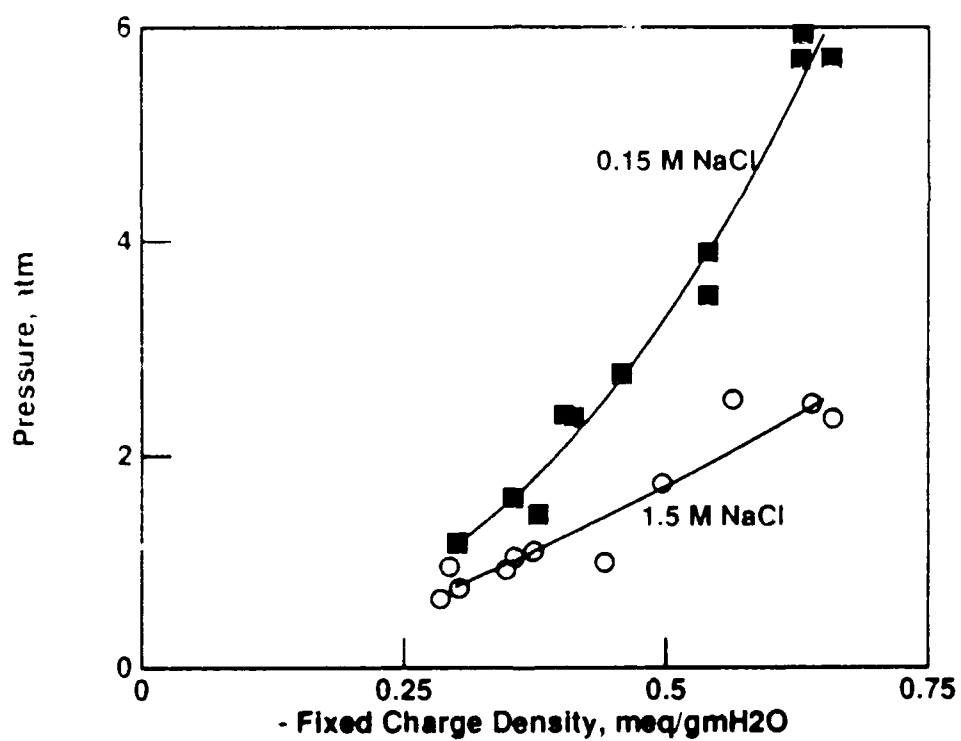


Figure 12. Polynomial fits to swelling pressure.

Swelling Pressure of CS vs FCD

Micromodel Fit

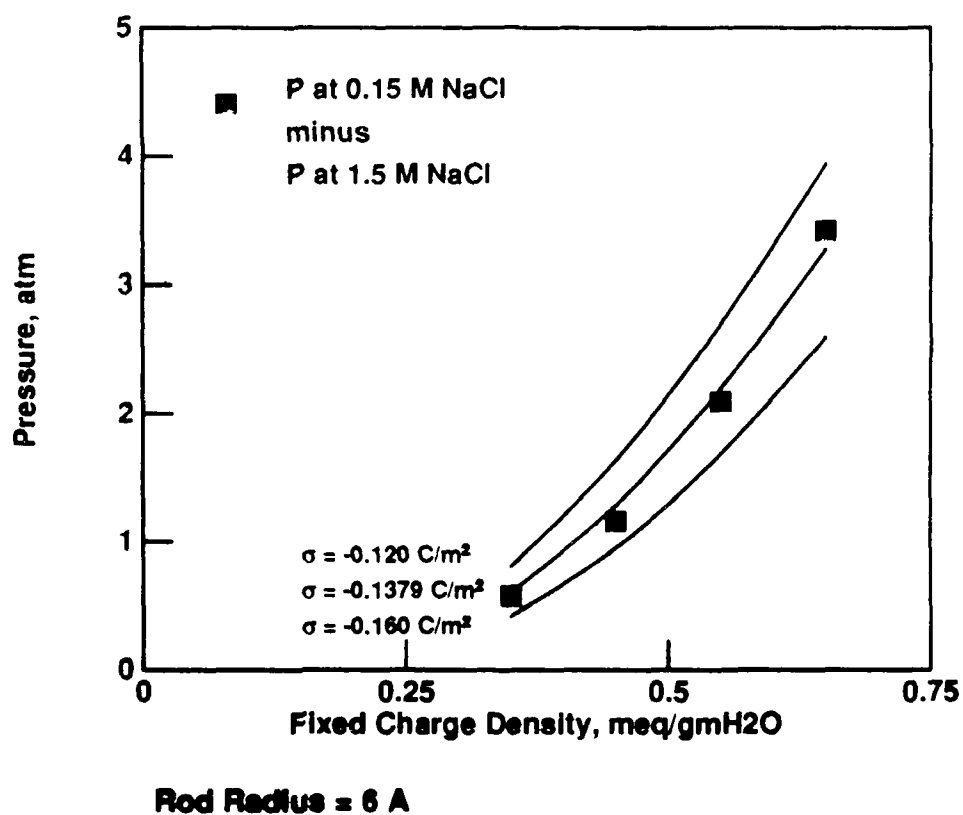


Figure 13. Micromodel fit to the electrostatic part of the swelling pressure.

freedom in the fit because variations in the 2d degree of freedom would not produce a significantly better chi (if standard deviations were available). Had other data been reported (such as hydration, which the procedures indicate was taken) another parameter (ex. \tilde{a}) could have been fixed by the experiment.

Here since there is effectively only 1 degree of freedom in the fit, the other must be chosen. Literature values indicate a hydrodynamic radius of 5–8.5 Å [51], whereas a value 9 Å was found to agree with measurements of hydraulic permeability and electrokinetic coefficients of cartilage [24]. Tables 3, 4, and 5 show that the data may be fit (by varying $\tilde{\sigma}$) with \tilde{a} satisfying any of these suggested values. It is pertinent to note that the quantity $(\tilde{b} - \tilde{a})$ was nearly constant for the different fits suggesting that, as far as swelling pressure is concerned, it is the separation distance of the charged surfaces that is most critical (not \tilde{a} or \tilde{b} separately), which could explain the degeneration from 2 to 1 degree of freedom.

Comparison to the Equilibrium Modulus of Articular Cartilage

The ionic strength dependence of the equilibrium modulus of articular cartilage is a manifestation of long-range electrostatic interactions [22]. At high ionic strength ($> 1M$) where long-range electrostatic interactions are shielded, the equilibrium modulus can be considered as arising from forces not accounted for in the unit cell PB approximation. As the ionic strength is lowered, the increase in modulus is interpreted as a result of the repulsion of fixed charge groups on the matrix. At physiological ionic strength (0.15M) the modulus is about twice that found at 1M (0.55 MPa, 0.27 MPa). With the assumption that the microstructure of the matrix does not change significantly as ionic strength is changed and can be adequately represented as the same unit cell, the ionic strength dependent contribution to the equilibrium modulus can be modelled as due to changes in the swelling pressure predicted by equation (33) in response to strain. Then

$$\tilde{H}_A^e = \tilde{H}_A - \tilde{H}_A^\infty \quad (64)$$

where \tilde{H}_A is the equilibrium modulus, \tilde{H}_A^e the electrostatic component, and \tilde{H}_A^∞ the equilibrium modulus at high ionic strength. In this section the model will be fit to the data of Figure 8, pg 156 of Eisenberg and Grodzinsky [22]. This data itself is a fit to descriptive functions not representing any model. The standard deviations are the deviations from this fit for 1 to 5 cartilage plugs 6.4 mm in diameter taken from the femoropatellar region of 2-year-old cattle.

The testing was done in a range of strain, 0% to 25%, so that the modulus from the unit cell is found here as

$$\tilde{H}_A^e = \frac{\tilde{P}_{swell}(.2) - \tilde{P}_{swell}(.1)}{0.1} \quad (65)$$

where $\tilde{P}_{swell}(.2)$ is the swelling pressure at 20% strain, $\tilde{P}_{swell}(.1)$ at 10% strain. One could choose different and multiple strains to find \tilde{H}_A^e , but the result would differ little. Equation(65) gives a modulus (independent of strain) valid in the strain range experimentally tested.

To find \tilde{H}_A^e , one must choose \tilde{a} , \tilde{b}_o (the unstrained cell boundary), and $\tilde{\sigma}$ as well as a model for strain. \tilde{a} is in the range $5 \rightarrow 8.5A^\circ$ [51]. Given the solid volume fraction of the GAG constituent V_s (Appendix) \tilde{b}_o can be found,

$$\tilde{b}_o = \tilde{a} \sqrt{\frac{1}{V_s}}. \quad (66)$$

$\tilde{\sigma}$ will be the fitted parameter. The strain will be modeled as shortening the outer cell diameter to \tilde{b} from the unstrained value \tilde{b}_o . Given a strain ϵ_G on the GAG constituent,

$$\tilde{b} = \tilde{b}_o(1 - \epsilon_G)^{1/2}. \quad (67)$$

The GAG strain is related to total tissue strain ϵ by

$$\epsilon_G = k\epsilon \quad (68)$$

where,

$$k = \frac{1 - V_S}{W_T} \quad (69)$$

and W_T is the fractional water content of the tissue as a whole (Appendix).

Choosing a rod radius of 6 Å, a solid volume fraction of 0.09, and $W_T = 0.8$ the best fit in Figure 14 was found by minimizing chi with respect to variations in $\bar{\sigma}$. The surface charge corresponds well with structural models of the chondroitin sulfate chain. The structural model predicts an intercharge spacing of $0.5nm \rightarrow 0.7nm$ [51, 52] whereas the surface charge found by the fit corresponds to spacing of $0.73nm$. The reasonable fit between theory and experiment suggests that electrostatic repulsion at the GAG chain level (as predicted by the PB equation) is the basis of the ionic strength dependent component of the equilibrium modulus.

EFFECT OF APPLIED ELECTRIC FIELDS

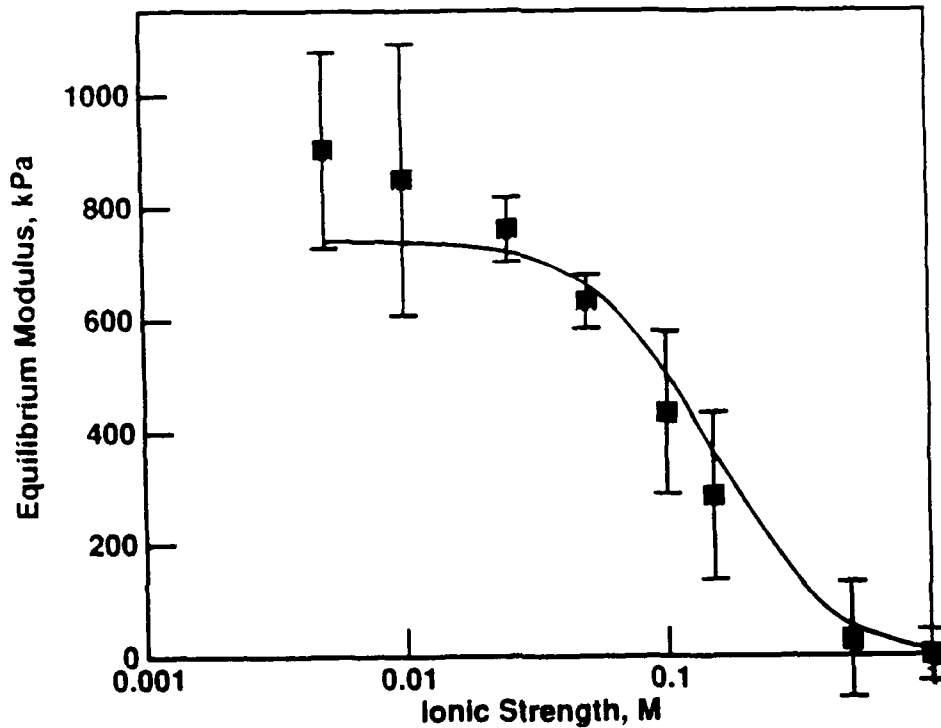
Experimental

Given the demonstrated development of a mechanically functional extracellular matrix, we have now begun a series of experiments to study the transduction mechanisms involved in response to electrical stimulation.

Initial studies have utilized Teflon chambers (Fig. 15) each of which contains two independent lanes capable of holding 16 cylindrical agarose/chondrocyte disks in each lane. Gel disks are placed into Teflon disk holders which, in turn, are inserted into the lanes as shown in Fig. 15. Two prototype chambers have now been constructed, but more will be needed. The disk holders will accept 3mm diameter by 1mm thick disks. (These chambers were constructed as part of a Bachelor's Thesis project by Paul M. Tiao, June 1989.) The lanes in the chambers are connected to platinum electrodes by means of "salt bridges" comprised of autoclavable plastic tubing filled with 5% w/v agarose. The electrode baths are filled with saline. This external electrode arrangement isolates the agarose/chondrocyte disks from any electrode reaction products. (Our previous experiments using cartilage organ culture explants showed that

Modulus (ES comp) vs. Ionic Strength

Micromodel Fit



Rod Radius = 6 Å

Cell Radius = 20 Å

Surface Charge = -0.0580 C/m^2

Chi = 2.51

Figure 14. Electrostatic component of articular cartilage equilibrium modulus micro-model fit to data of Figure 8, pg 156 of Eisenberg and Grodzinsky 1985.

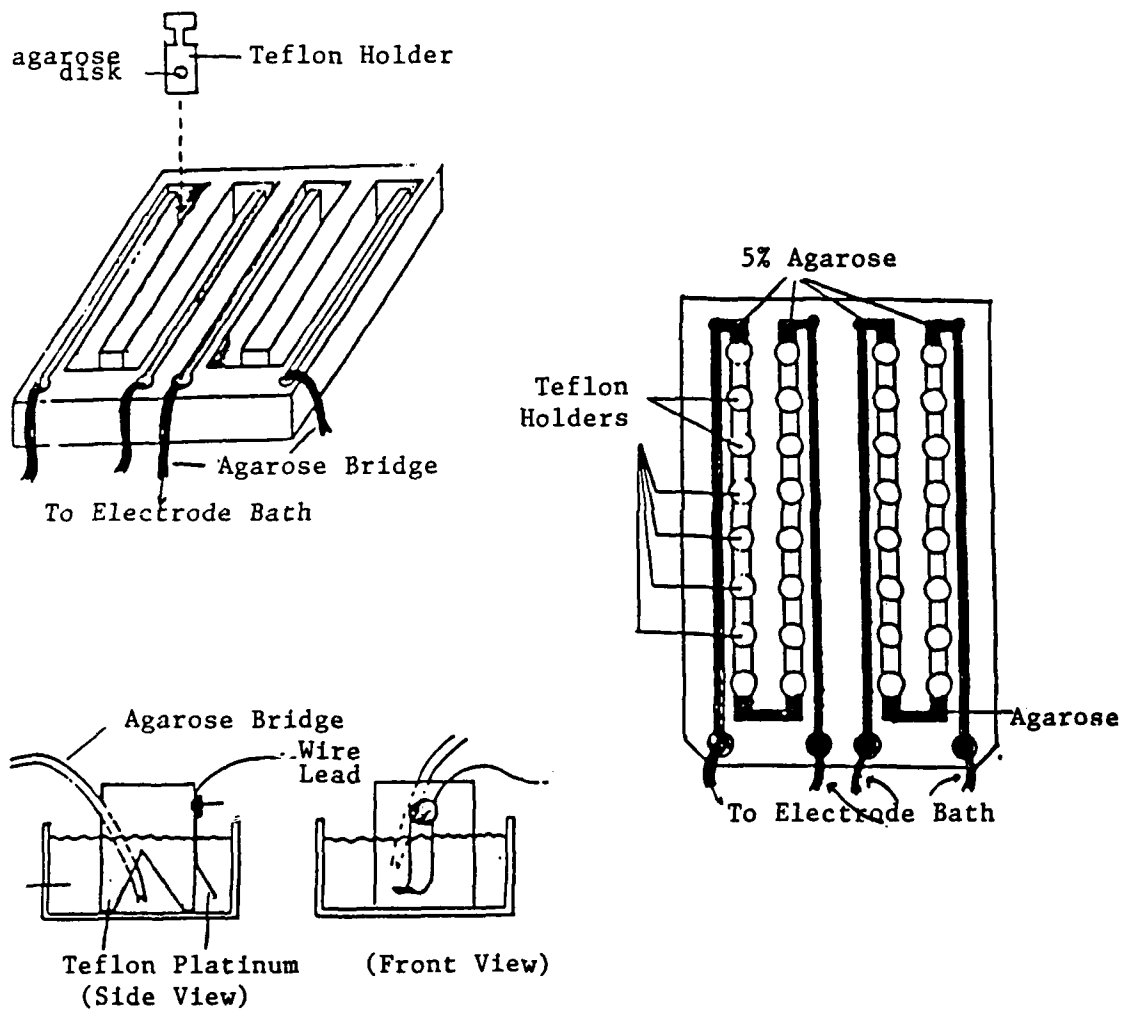


Figure 15. Electrical Stimulation Chamber.

such electrode reaction products could themselves stimulate the synthesis of stress response proteins in the cartilage.)

Further work will have to be done to quantify temperature at various locations within the stimulation chamber. Previous tests of this system have shown that negligible ohmic heating occurs for current densities up to 10-20 mA/cm²; feedback-controlled circulating cooling fluid may be needed for higher current densities.

Since it is absolutely essential that temperature, field and current parameters be continuously monitored and recorded throughout each test, a dedicated microcomputer system will have to be developed for this purpose.

A preliminary experiment on the effect of electrical currents on sulfate and proline incorporation for day 32 plugs is shown in Fig. 15.

While radiolabel incorporation appears to change with applied current density, additional experiments will have to be performed to confirm this result.

Electrical Stimulation at 100 Hz

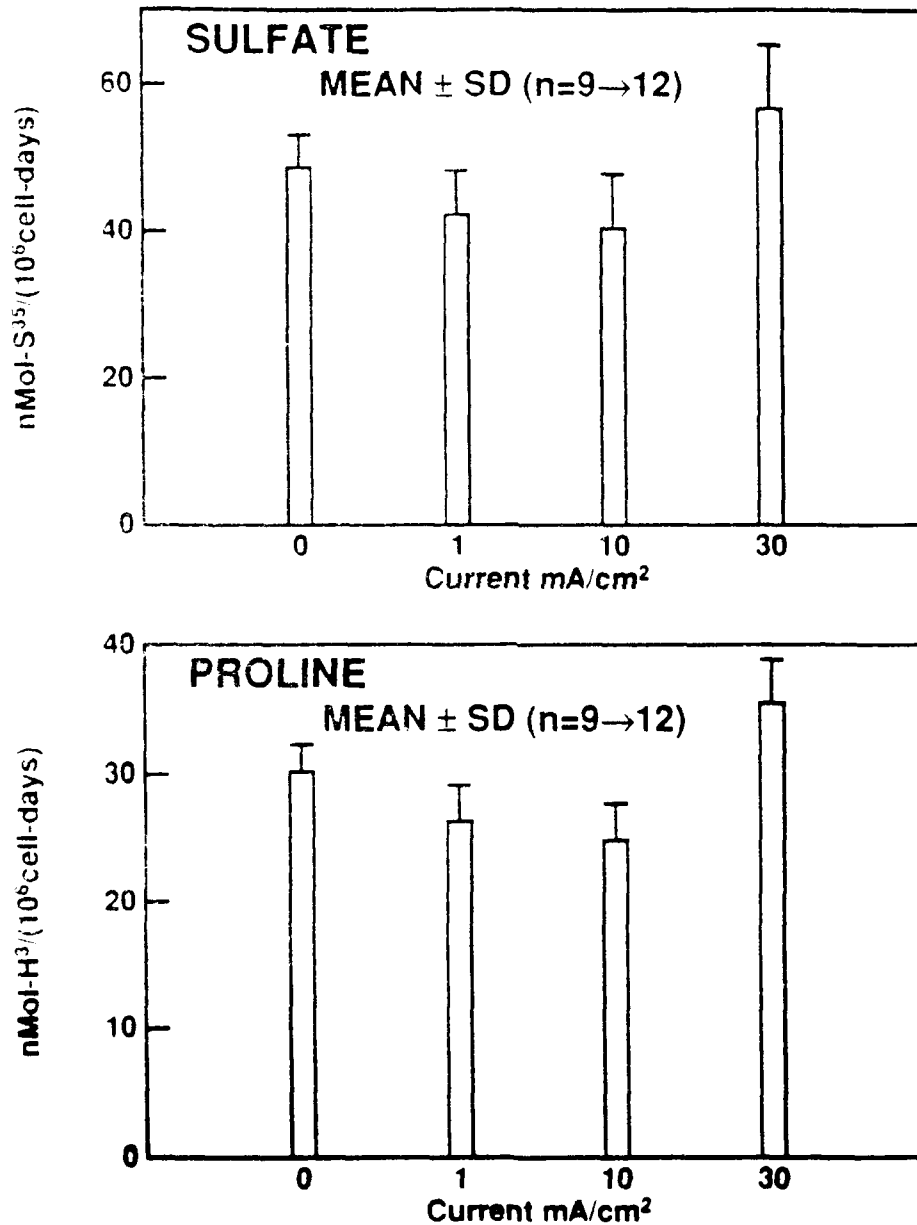


Figure 16. Electrical Stimulation at 100 Hz of 3mm Chondrocyte/Agarose plugs from day 32 and its Effect on Proline and Sulfate Incorporation.

References

- [1] H J Mankin and K D Brandt. Biochemistry and metabolism of cartilage in osteoarthritis. In Howell RW, editor, *Osteoarthritis*, pages 43-79, WB Saunders, Philadelphia, 1984.
- [2] A Maroudas. Physico-chemical properties of articular cartilage. In M A R Freeman, editor, *Adult Articular Cartilage*, 2nd ed., pages 215-290, Pitman, Tunbridge Wells, England, 1979.
- [3] V C Mow, M H Holmes, and W M Lai. Fluid transport and mechanical properties of articular cartilage: a review. *J Biomechanics*, 17:377-394, 1984.
- [4] W A Hodge, R S Fijan, K L Carlson, R G Burgess, W H Harris, and R W Mann. Contact pressures in the human hip joint measured in vivo. *Proc Natl Acad Sci USA*, 83:2879-2883, 1986.
- [5] A J Grodzinsky. Electromechanical and physicochemical properties of connective tissue. *CRC Crit Rev Bioeng*, 9:133-199, 1983.
- [6] B Caterson and D A Lowther. Changes in the metabolism of the proteoglycans from sheep articular cartilage in response to mechanical stress. *Biochim Biophys Acta*, 540:412-422, 1978.
- [7] M J Palmoski, E Perricone, and K D Brandt. Development and reversal of a proteoglycan aggregation defect in normal canine knee cartilage after immobilization. *Arthritis Rheum*, 22:508-517, 1979.
- [8] K E Kuettner, R Schleyerbach, and Hascall V C. *Articular Cartilage Biochemistry*. Raven Press, New York, NY, second edition, 1986.
- [9] R Schneiderman, D Keret, and A Maroudas. Effects of mechanical and osmotic pressure on the rate of glycosaminoglycan synthesis in the human adult femoral head cartilage: an in vitro study. *J Orthop Res*, 4:393-408, 1986.

- [10] M L Gray, A M Pizzanelli, A J Grodzinsky, and R C Lee. Mechanical and physicochemical determinants of the chondrocyte biosynthetic response. *J Orthop Res*, 6:111-119, 1988.
- [11] R L Sah, J Y H Doong, Y J Kim, A J Grodzinsky, A H K Plaas, and J D Sandy. Biosynthetic response of cartilage explants to mechanical and physicochemical stimuli. *Orthop Trans*, 12:330-331, 1988.
- [12] M B Aydelotte, R Schleyerbach, B J Zeck, and Kuettner K E. Articular chondrocytes cultured in agarose gel for study of chondrocytic chondrolysis. In K E Kuettner, editor, *Articular Cartilage Biochemistry*, pages 235-257, Raven Press, New York, NY, 1986.
- [13] M B Aydelotte and K E Kuettner. Differences between sub-populations of cultured bovine articular chondrocytes. I. morphology and cartilage matrix production. *Connective Tissue Research*, 18:205-222, 1988.
- [14] M B Aydelotte, R R Greenhill, and K E Kuettner. Differences between sub-populations of cultured bovine articular chondrocytes. II. proteoglycan metabolism. *Connective Tissue Research*, 18:223-234, 1988.
- [15] P D Benya and J D Shaffer. Dedifferentiated chondrocytes reexpress the differentiated collagen phenotype when cultured in agarose gels. *Cell*, 30:215-224, 1982.
- [16] A L Aulthouse, M Beck, E Griffey, J Sanford, K Arden, M A Machado, and W A Horton. Expression of the human chondrocyte phenotype in vitro. *In Vitro Cellular and Developmental Biology*, 25:659-668, 1989.
- [17] D Sun, M B Aydelotte, B Maldonado, K E Kuettner, and J H Kimura. Clonal analysis of the population of chondrocytes from the swarm rat chondrosarcoma in agarose culture. *J Orthop Res*, 4:427-436, 1986.

- [18] K E Kuettner, V A Memoli, B U Pauli, N C Wrobel, E J-M A Thonar, and J C Daniel. Synthesis of cartilage matrix by mammalian chondrocytes in vitro. *II. maintenance of collagen and proteoglycan phenotype. J Cell Biol*, 93:751-757, 1982.
- [19] P D Benya, P D Brown, and S R Padilla. Microfilament modification by dihydrocytochalasin B causes retinoic acid-modulated chondrocytes to reexpress the differentiated collagen phenotype without a change in shape. *J Cell Biol*, 106:161-170, 1988.
- [20] P D Brown and P D Benya. Alterations in chondrocyte cytoskeletal architecture during phenotypic modulation by retinoic acid and dihydrocytochalasin b-induced reexpression. *J Cell Biol*, 106:171-179, 1988.
- [21] A Lindahl, A Nilsson, and O G P Isaksson. Effects of growth hormone and insulin-like growth factor-i on colony formation of rabbit epiphyseal chondrocytes at different stages of maturation. *J Endocr*, 115:263-271, 1987.
- [22] S R Eisenberg and A J Grodzinsky. Swelling of articular cartilage and other connective tissues. *J Orthop Res*, 3:148-159, 1985.
- [23] E H Frank and A J Grodzinsky. Cartilage electromechanics-II. a continuum model of cartilage electrokinetics and correlation with experiments. *J Biomechanics*, 20:629-639, 1987.
- [24] S R Eisenberg and A J Grodzinsky. Electrokinetic micromodel of extracellular matrix and other polyelectrolyte networks. *Physicochemical Hydrodynamics*, 10:517-539, 1988.
- [25] Helfferich. *Ion Exchange*. McGraw-Hill, New York, NY, 1962.
- [26] A Maroudas. Physical chemistry of articular cartilage and the intervertebral disc. In L Sokoloff, editor, *The Joints and Synovial Fluid, Vol. II*, pages 239-291, Academic Press, New York, 1980.

- [27] J P G Urban, A Maroudas, M T Bayliss, and J Dillon. Swelling pressures of proteoglycans at the concentrations found in cartilagenous tissues. *Biorheology*, 16:447-464, 1979.
- [28] J D Wells. Salt activity and osmotic pressure in connective tissue. I. a study of solutions of dextran sulphate as a model system. *Proc R Soc Lond B*, 183:399-419, 1973.
- [29] B N Preston, J M Snowden, and K T Houghton. Model connective tissue systems: the effect of proteoglycans on the distribution of small non-electrolytes and micro-ions. *Biopolymers*, 11:1645-1659, 1972.
- [30] G S Manning. Limiting laws and counterion condensation in polyelectrolyte solutions I. colligative properties. *J Chem Phys*, 51:924-933, 1969.
- [31] J D Wells. Thermodynamics of polyelectrolyte solutions. an empirical extension of the manning theory to finite salt concentrations. *Biopolymers*, 12:223-227, 1973.
- [32] I H M Muir. Biochemistry. In M A R Freeman, editor, *Adult Articular Cartilage*, 2nd ed., pages 145-214, Pitman, Tunbridge Wells, England, 1979.
- [33] E B Hunziker and R K Schenk. Structural organization of proteoglycans in cartilage. In T N Wight and R P Mecham, editors, *Biology of Proteoglycans*, pages 155-185, Academic Press, New York, NY, 1987.
- [34] P G de Gennes. Global molecular shapes in polyelectrolyte solutions. In D H Everett and B Vincent, editors, *Colston Papers No. 29. Ions in Macromolecular and Biological Systems.*, pages 155-185, Scientechnica, Bristol, UK, 1978.
- [35] R L-Y Sah, Y-J Kim, J-Y H Doong, A J Grodzinsky, A H K Plaas, and J D Sandy. Biosynthetic response of cartilage explants to dynamic compression. *J Orthop Res*, 7:619-636, 1989.

- [36] R W Farndale, D J Buttle, and A J Barrett. Improved quantitation and discrimination of sulphated glycosaminoglycans by use of dimethylmethylene blue. *Biochim Biophys Acta*, 883:173-177, 1986.
- [37] E H Frank and A J Grodzinsky. Cartilage electromechanics-I. electrokinetic transduction and the effects of electrolyte pH and ionic strength. *J Biomechanics*, 20:615-627, 1987.
- [38] Y J Kim, R L Y Sah, J Y H Doong, and A J Grodzinsky. Fluorometric assay of DNA in cartilage explants using Hoechst 33258. *Anal Biochem*, 174:168-176, 1988.
- [39] R M Fuoss, A Katchalsky, and S Lifson. The potential of an infinite rod-like molecule and the distribution of counterions. *Proc Nat Acad Sci (U.S.)*, 37:579-589, 1951.
- [40] R A Marcus. Calculation of thermodynamic properties of polyelectrolytes. *J Chem Phys*, 23:1057-1068, 1955.
- [41] H Wennerstrom, B Jonsson, and P Linse. The cell model for polyelectrolyte systems. exact statistical mechanical relations, Monte Carlo simulations, and the Poisson-Boltzmann approximation. *J Chem Phys*, 76:4665-4670, 1982.
- [42] S L Carnie and G M Torrie. Statistical mechanics of the electrical double layer. *Adv. in Chem Phys*, 56:141-253, 1984.
- [43] S McLoughlin. The electrostatic properties of membranes. *Ann Rev Biophys Biophys Chem*, 89:113-136, 1989.
- [44] B Jonsson, H Wennerstrom, and B Halle. Ion distributions in lamellar liquid crystals. a comparison between results from Monte Carlo simulations and solutions of the Poisson-Boltzmann equation. *J Phys Chem*, 84:2179-2185, 1980.

- [45] F Oosawa. *Polyelectrolytes*. Marcel Dekker, Inc., New York, NY, first edition, 1971.
- [46] M Fixman. The Poisson-Boltzmann equation and its application to polyelectrolytes. *J Chem Phys*, 70:4995-5005, 1979.
- [47] B H Zimm and M Le Bret. Counter-ion condensation and system dimensionality. *J Biomolecular Structure and Dynamics*, 1:461-471, 1983.
- [48] J S McCaskill and E D Fackerell. Painleve solution of the Poisson-Boltzmann equation for a cylindrical polyelectrolyte in excess salt solution. *J Chem Soc Faraday Trans 2*, 84:161-179, 1988.
- [49] Y Gur, I Ravina, and A J Babchin. On the electrical double layer theory I. a numerical method for solving a generalized Poisson-Boltzmann equation. *J Coll Int Sci*, 64:326-332, 1978.
- [50] A Katchalsky and P F Curran. *Nonequilibrium Thermodynamics in Biophysics*. Harvard University Press, Cambridge, MA, first edition, 1967.
- [51] W D Comper and Laurent T C. Physiological function of connective tissue polysaccharides. *Physiological Reviews*, 58:255-315, 1978.
- [52] K H Parker, C P Winlove, and A Maroudas. The theoretical distributions and diffusivities of small ions in chondroitin sulphate and hyaluronate. *Biophysical Chemistry*, 32:271-282, 1988.
- [53] M Venn and A Maroudas. Chemical composition and swelling of normal and osteoarthrotic femoral head cartilage. I. chemical composition. *Annals of the Rheumatic Diseases*, 36:121-129, 1977.
- [54] I H M Muir. The chemistry of the ground substance of joint cartilage. In L Sokoloff, editor, *The Joints and Synovial fluid*, pages 27-94, Academic Press, New York, 1980.

- [55] M D Gryn timer, D R Eyre, and D A Kirschner. Collagen type 2 differs from type 1 in native molecular packing. *Biochem Biophys Acta*, 626:346-355, 1980.

APPENDIX

CARTILAGE PARAMETERS

Cartilage Constituent Compartments

To implement the unit cell to describe cartilage properties, an account must be made of the various constituents of cartilage, namely the GAG constituent as represented by the unit cell, and everything else (collagen etc.). There is both solid and fluid in each giving rise to four distinguished volume fractions :

$$\begin{aligned} S_G & - \text{ gag solid} \\ W_G & - \text{ gag water} \\ S_O & - \text{ other solid} \\ W_O & - \text{ other water} \end{aligned}$$

Only 3 equations are independent since they sum to 1. Combinations of the 3 are available from the literature,

$$W_T = W_G + W_O = .70 \rightarrow .80 \quad (70)$$

53, 54 ,

$$f_{ow} = \frac{W_O}{W_T} \cong .35 \quad (71)$$

55],

$$f_{GS} = \frac{S_G}{S_O + S_G} \cong .15 \rightarrow .25. \quad (72)$$

For model implementation the following 3 parameters (and their ranges from above) are most useful,

$$W_T = .70 \rightarrow .80 \quad (73)$$

$$f_{GW} = \frac{W_G}{W_T} = 1 - f_{ow} = .6 \rightarrow .7 \quad (74)$$

$$V_S = \frac{S_G}{W_G} = \frac{(1 - W_T)f_{GS}}{W_T(1 - f_{OW})} = .05 \rightarrow .18 \quad (75)$$

Strain in GAG Compartment

The strain in the GAG constituent is more than that of the total tissue due to its higher water content. With the assumption that f_{GW} (or f_{OW}) is constant while fluid is lost from the tissue during strain,

$$\frac{\epsilon_G}{\epsilon} = \frac{1 - V_S}{W_T} \quad (76)$$

Where ϵ is the total tissue strain and ϵ_G is the strain on the GAG constituent. For example, when all the fluid is excluded, $\epsilon = W_T \simeq 0.8$ and $\epsilon_G = 1 - V_S \simeq 0.92$ and only the solid remains.